INVESTIGATING THE FORMATION AND EVOLUTION OF MEGA-PALEOLAKES IN THE MIDDLE KALAHARI OF SEMI-ARID BOTSWANA FROM SEDIMENTARY AND GEOCHEMICAL PROXIES

By

MORGAN OSTROSKI

Bachelor of Science in Geology

Mercyhurst College

Erie, PA

2011

Submitted to the Faculty of the
Graduate College of the
Oklahoma State University
in partial fulfillment of
the requirements for
the Degree of
MASTER OF SCIENCE
May, 2013

INVESTIGATING THE FORMATION AND EVOLUTION OF MEGA-PALEOLAKES IN THE MIDDLE KALAHARI OF SEMI-ARID BOTSWANA FROM SEDIMENTARY AND GEOCHEMICAL PROXIES

Thesis Approved:

Dr. Eliot Atekwana

Thesis Adviser

Dr. Tracy Quan

Dr. Joseph Donoghue

ACKNOWLEDGEMENTS

I would like to start by acknowledging my advisor Dr. Eliot Atekwana. He spent countless hours helping me with lab analyses as well as helping me write my thesis. I would not be where I am today without his constant coaching and availability. I want to thank my committee members Dr. Tracy Quan and Dr. Joseph Donoghue. They gave me critique and input to make my thesis better. I appreciate their activeness throughout the process. I also want to thank our Geochemistry Lab Tech, Christopher Geyer who gave me constant guidance and help.

Next, I want to acknowledge my family and friends. My family supported me from New York my whole time here in Oklahoma. My parents, grandparents, and sister have always been there for me and had faith in my ability to accomplish my goals here at Oklahoma State University. I would not be here without their constant encouragement and support.

To my Oklahoma State family: Natalie Gentry, Keith Rivera, Erin Roehrig, Stephanie LeBlanc, Jason Hanzel, Sara Callner, Sahar Mohammadi, Jared Morris, Jake Carter, Pride Abongwa, Rawlings Akondi, Joe Dixon, Jason Baugh and so many more, I have had the greatest experience here because of you guys. All the faculty, staff, and students at the Boone Pickens School of Geology have made my time here an amazing experience. The classes and opportunities that are provided in the geology department have prepared me for a career as a professional geologist at EOG Resources.

Lastly, I want to acknowledge my future employer EOG Resources who gave me an amazing opportunity as an intern the summer of 2012. I learned how to apply my knowledge of geology in a professional manner and apply it to explore for petroleum resources. EOG has supported me and encouraged me since I began my internship. My experience so far has been extremely positive and I look forward to beginning my career with EOG upon graduation.

Name: Morgan Ostroski

Date of Degree: May, 2013

Title of Study: INVESTIGATING THE FORMATION AND EVOLUTION OF MEGA-PALEOLAKES IN THE MIDDLE KALAHARI OF SEMI-ARID BOTSWANA FROM SEDIMENTARY AND GEOCHEMICAL PROXIES

Major Field: Geology

We investigated the occurrence and evolution of mega-paleolakes in the middle Kalahari Desert in semi-arid Botswana, Africa based on sedimentary and geochemical proxies. The mega-paleolakes covered more than 60,000 km^2 including the present day lower Okavango Delta. This study tested the following working hypotheses (1) environmental conditions leading to the formation of mega-paleolakes and their presence is recorded in sediments of the lower Okavango Delta and can be used to distinguish between lacustrine and fluvial paleoenvironments and (2) more than one paleolake episode will be recorded as lacustrine sedimentation either separated by a disconformity or by fluvial sedimentation. The objectives of the study were to collect sediments from an area of the delta projected to be covered by the mega-paleolake, conduct stratigraphic, geochemical and stable isotope measurements, and evaluate the data for the presence and evolution of a mega-paleolake beyond the present day lake basin settings. Results of the study indicate a possible mega-paleolake in the stratigraphic record based on anomalously high concentrations of total inorganic carbon, suggesting local and regional wet climate. The development of mega-lakes has major ramifications for people and infrastructure of the Okavango Delta as such a reoccurrence in modern times can cause devastation to the region.

TABLE OF CONTENTS

Chapter Page

LIST OF TABLES

Table Page

LIST OF FIGURES

Figure Page

CHAPTER I

INTRODUCTION

1.1 Project Motivation

We investigated the existence and evolution of mega-paleolakes in the Middle Kalahari desert in Botswana, Africa based on sedimentary and geochemical proxies. The mega-paleolakes covered more than 60,000 km^2 and extended beyond the present day Makgadikgadi, Ngami and Mababe lake basins, as well as much of the lower Okavango Delta (Shaw, 1988). Previous studies suggest that there may have been two episodes of mega-paleolake formation; an earlier paleolake Makgadikgadi which was followed by paleolake Thamalakane (Shaw, 1988). The occurrence of mega-paleolakes and the climatic history of this region were initially inferred from elevations of shorelines of lake high stands from the Makgadikgadi, Ngami and Mababe lake basins (Shaw et al., 2003). Beach ridges associated with lake high stands of paleolake Makgadikgadi occur at elevations of 945 m above sea level (asl) and those associated with paleolake Thamalakane occur at 936 m asl (Shaw et al., 2003; Burrough and Thomas, 2008; Burrough et al., 2009a; 2009b).

One problem with the use of beach ridges associated with lake high stands is that they do not provide a temporal history of the lake evolution from sedimentation. Additionally, fluctuations in the lake levels may erode beach ridges of lower high stands from beach ridge records. Even though the temporal history of lake sedimentation and climate change can be inferred from in-lake sedimentation, this does not provide insights into the spatial extent of and the behavior of the mega-paleolake beyond the lake basin.

Although the mega-paleolakes extended beyond the present-day Makgadikgadi, Ngami and Mababe lake basins (Burrough and Thomas, 2008), there are limited studies that investigate the occurrence of a mega-paleolake outside these lake basins. Fields (2012) studied sedimentary, geochemical, and isotopic proxies at the distal edge of the Okavango Delta on the downthrown side of the Thamalakane fault. Fields (2012) showed that the sediments collected at an elevation of 940 m asl showed evidence of lacustrine deposits which was attributed to the presence of a mega-paleolake. The Field (2012) study was designed to assess the possibility of sedimentation associated with a lake that formed above the 940 m asl elevation, and thus does not provide information about the possibility of a mega-paleolake at a lower high stand.

Sedimentary, geochemical, and isotopic proxies are used to reconstruct paleoenvironments. Sedimentary proxies such as the proportion of sand, silt, clay, graphic skewness, graphic mean and sorting can be used to distinguish among aeolian, fluvial and lacustrine depositional environments (Friedman, 1967). However, if the stratigraphic units have been altered and/or influenced by more than one depositional process, sedimentary proxies alone cannot be used to identify a mega-paleolake. Geochemical and isotopic proxies can be used to further define lacustrine sedimentation.

Geochemical proxies may help signify presence or absence of the mega-paleolakes by confirming lacustrine sedimentation obtained from sedimentary proxies.

During the deposition of sediments, carbonates and organic matter can be transported from the watershed and deposited along with the sediments. In settings where the deposition occurs in lakes, additional carbonates can be precipitated from solution if chemical saturation with respect to carbonate occurs (Dean and Fouch, 1983). Aquatic plants which grow in a lake can also be deposited as part of the sedimentary record (Meyers and Teranes, 2001). Biogenic silica deposition may result from *in situ* growth of diatoms in a lake. Thus, inorganic carbon, organic carbon and biogenic silica deposition can be autochthonous or allochthonous (Dean and Fouch, 1983).

Stable carbon ($\delta^{13}C$) and oxygen isotopes ($\delta^{18}O$) can be used to assess the source of carbonates. Variations in the $\delta^{13}C$ of inorganic carbon can be related to differences in the sources of carbonate supplied from the watershed to the sedimentary basin or to isotopic fractionation during precipitation of the carbonates formed from aqueous solution (Emrich et al., 1970). The geochemical proxies: total inorganic carbon (TIC), $\delta^{13}C$ of inorganic carbon, $\delta^{18}O$ of inorganic carbon, total organic carbon (TOC), and biogenic silica provide useful data to evaluate the formation of a lake at the distal portion of the Okavango Delta from the sedimentary record at the study site.

Combining sedimentary and geochemical analysis of the sediments will provide an interpretation of the data to determine the presence of a mega-paleolake and how many episodes of mega-paleolake formation occur within the sedimentary record. We have developed a working conceptual model of how single or multiple episodes of mega-

paleolake formation are recorded in the sedimentation of the lower Okavango Delta (Fig. 1). We will determine if the mega-paleolake(s) occurred across the lower Okavango Delta by seeking evidence of one or more episodes of lake deposits within the sedimentary record of the lower Okavango Delta.

1.2 Conceptual Models

The geomorphology of the lower Okavango Delta where the study site resides is presently elevated compared to other areas at the base of the delta (Fig. 2). There is approximately 9 meters difference in elevation from the base of the delta where the rivers flow to the location of the study site according to elevation data from Google Earth. Therefore, it is not normally flooded by rivers, and so flooding of the area would be due to mega-lake formation or periods of high discharge by the rivers. Mega-lakes have formed along the upthrown side of the Thamalakane fault. If a mega-lake formed at the study site, the lake will have to have extended into the lower delta on the downthrown side of the fault and the study location will record lacustrine sedimentation. The sedimentary record of the lower Okavango Delta will record the hydrology of the lake by providing evidence of the wet climate during mega-lake formation or dry climate that led to demise of a mega-lake.

Conceptual models of sedimentation in the lower Okavango Delta that show fluvial and lacustrine deposition are presented in Figure 1. In panel A (Fig. 1), the region is first covered by sediment, most likely fluvial in origin, pre-dating mega-lake sedimentation. Then a mega-lake is formed from flooding along the upthrown side of the fault, and produces lacustrine sedimentation. Over time the lake disappears due to

changes in hydrology or climate, and the region is covered in post-lake fluvial sedimentation. This model shows a single episode of a mega-paleolake. Panel B (Fig. 1) shows a similar scenario to panel A (Fig. 1). However, after fluvial and lacustrine deposition from the first mega-lake, a second lake is formed. Therefore, 2 episodes of recording the presence of mega-paleolakes are represented in the sedimentary record.

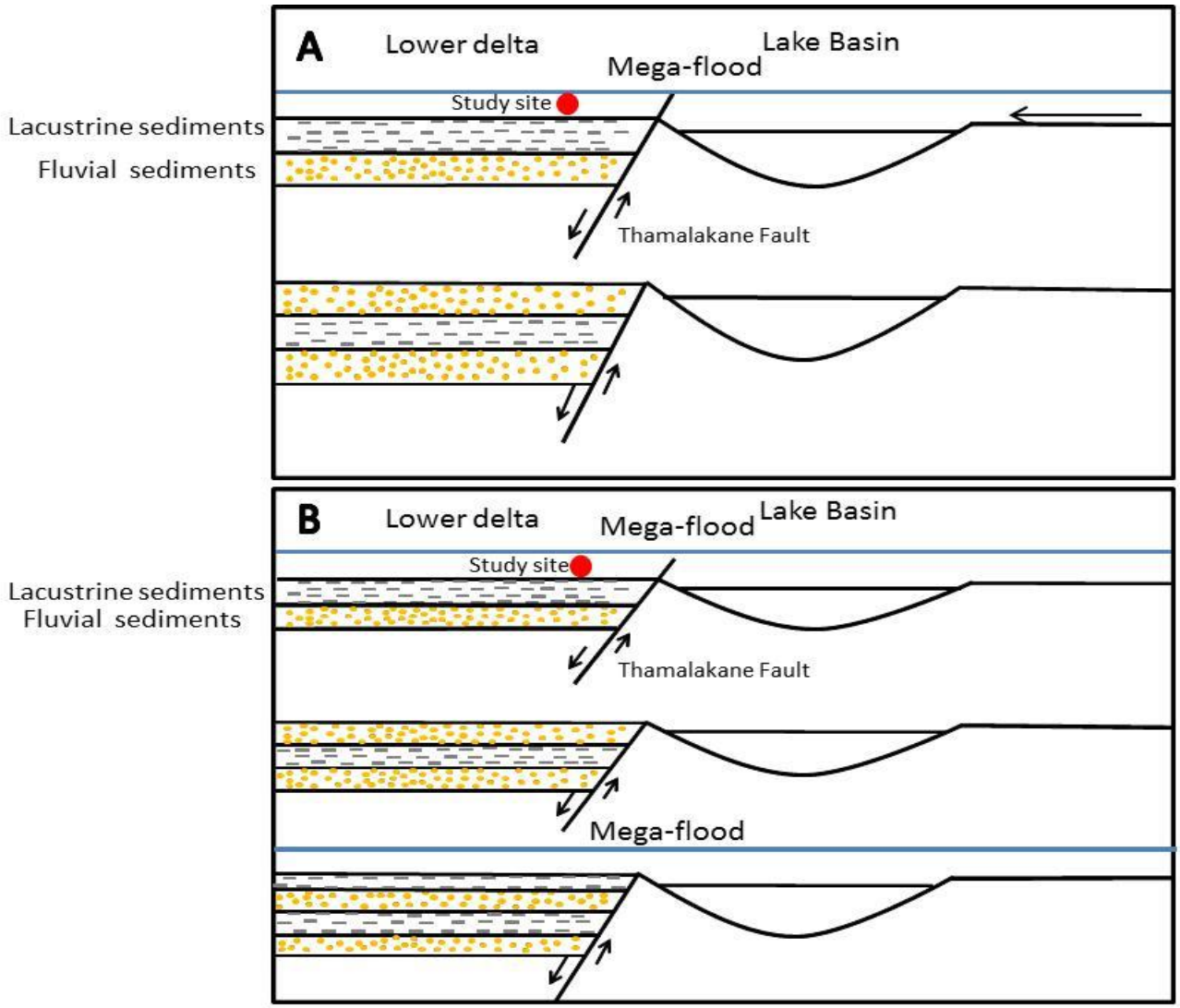

Fig. 1: Conceptual model showing 2 scenarios. Scenario A illustrates 1 episode of a mega-paleolake and scenario B indicates more than 1 episode of a mega-paleolake.

The conceptual model illustrates the presence of lacustrine sedimentation and fluvial deposition. However, it is not constrained by age, so only the relative timing of the events can be established. The lake sediments across the lake basin are time equivalent because they cover the region at one time period; however, the same cannot be said for the fluvial deposits. There may also be unconformities due to non-deposition or erosion which may erode lacustrine deposits, so that the stratigraphic record may not necessarily record the evidence of lakes.

1.3 Hypotheses and Project Objectives

The overarching goal of this project is to determine the presence and evolution of mega-paleolakes in the lower Okavango Delta. This study is conducted away from the present day lake basins in the Middle Kalahari and is focused in the lower portion of the Okavango Delta within the area suggested to have been occupied by a mega-paleolake (Shaw, 1988). This study tested the following working hypotheses (1) environmental conditions leading to the formation of a mega-paleolake and its presence are recorded in sediments of the lower Okavango Delta and can be used to distinguish between lacustrine and fluvial paleoenvironments and (2) more than one paleolake episode will be recorded as lacustrine sedimentation either separated by a disconformity or by fluvial sedimentation. The second hypothesis assumes that the process of fluvial deposition is independent of the conditions that lead to the formation of a mega-lake.

The objectives of this study were to (1) assess sedimentary, geochemical and isotopic proxies in the near-surface sediments (< 7 m) in the lower Okavango Delta for evidence of the presence of lacustrine sedimentation associated with a mega-paleolake

and (2) to evaluate the proxy data for the relative timing and evolution of single or multiple episodes of mega-paleolakes in this region.

To accomplish the study objectives, we (1) collected sediments from an area of the lower Okavango Delta projected to be covered by mega-paleolakes, (2) conducted stratigraphic, geochemical and stable isotope measurements and (3) evaluated the data for the presence and evolution of mega-paleolakes.

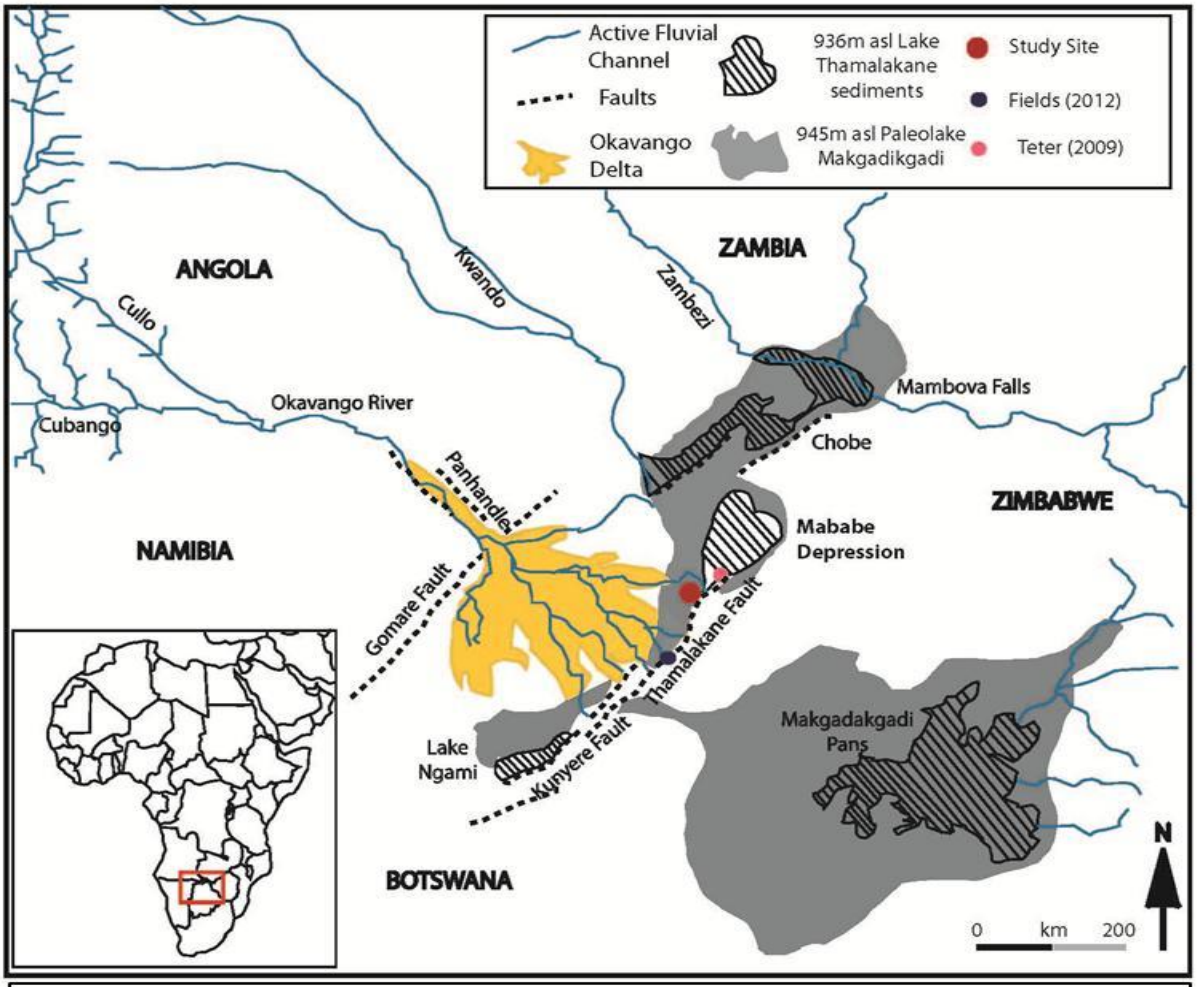

Fig. 2: Map showing extent of paleolakes in the Okavango Delta, and the location of the study site and previous studies in the Kalahari (modified from Burrough and Thomas (2008)).

1.4 Project Significance

We anticipate that the presence of lacustrine deposits within the sedimentary section in the lower Okavango Delta that will confirm the existence of a mega-paleolake that extended between the Lake Mababe depressions, Lake Ngami basin and the Makgadikgadi basin. The presence of mega-paleolakes in this region is important for envisioning the impacts of future climate change on settlements, infrastructure and human activities in the region (Hamandawana et al., 2008). Flooding from a future mega-lake can displace people, destroy infrastructure and alter tourism. This may result in relocation for the society. It can also affect plant and animal communities that exist in the area by creating inhabitable conditions.

Understanding the creation and demise of previous mega-lakes in this area can also be useful for future studies. The data from this research can be incorporated into rainfall and flooding models of the area. Incorporating the lifespan of the mega-paleolakes with rainfall and flooding models of the area can help predict landscape changes due to climate changes, which is beneficial to society. The principle of uniformitarianism must be applied to areas, such as northern Botswana, with the potential of repetition of past environmental change. We can interpret the past and examine environmental changes such as climate and use the result for future planning.

CHAPTER II

BACKGROUND

2.1 Regional Framework

The Okavango Delta in Northern Botswana (Fig. 2) is about 22,000 km^2 in area and is located in a semi-arid environment. The Okavango Delta consists of a Panhandle and delta portion (McCarthy and Ellery, 1998). The delta portion is an alluvial fan hosted within a nascent rift, the Okavango Rift Zone (ORZ) (e.g. Stanistreet and McCarthy, 1993; McCarthy and Ellery, 1998; Kinabo et al., 2007; Bufford et al., 2012), a southwest extension of the East Africa Rift system (EARS). The ORZ is bound to the northwest by the Gomare fault and to the southwest and northeast by the Kunyere and Thamalakane faults (McCarthy and Ellery, 1998; Modisi et al., 2000; Kinabo et al., 2007). The ORZ is a 120 km wide SE-dipping rollover half-graben caused by an east-west extension, and filled with lacustrine and deltaic sediments (Bufford et al., 2012).

2.2 Hydrology and Lacustrine History

The existence of mega-paleolakes (Fig. 2) in the middle Kalahari has been strongly influenced by tectonic activities. In the final division of Gondwanaland during the mid-Jurassic, southern Africa was uplifted creating the Great Escarpment

(Thomas and Shaw, 1988). This resulted in a gently down warped basin which created a framework for the drainage patterns in the Kalahari (Thomas and Shaw, 1988). The Okavango River is the only major river that remains today (Thomas and Shaw, 1988). The major development of the Okavango Delta, and its surrounding basins, began to occur during the Cretaceous (Goudie, 2004). During the late to middle Cretaceous, the Karoo and Kalahari were the two main rivers draining watersheds in southern Africa, which extends into Botswana (Goudie, 2004). During the Late Cretaceous, block-faulting in northern Botswana and subsidence of the Kalahari basin impounded the Okavango River which allowed for the formation of large lakes, and also the deposition of the Kalahari Basin sediments (Haddon and McCarthy, 2005).

Formation of the lakes is driven by climate and drainage evolution. Previous paleolake Makgadikgadi was initiated 42,000 to 40,000 years ago (Huntsman-Mapila et al., 2006), and paleolake Thamalakane existed 17,000 to 12,000 years ago (Shaw, 1988). Tropical winds from the Atlantic and easterly winds from the Indian Ocean are sources of moisture to the Middle Kalahari environment (Burrough et al., 2009). The amount of precipitation was vital to formation of the mega-paleolakes and depends on the position of the Inter Tropical Convergence Zone (ITCZ). This in turn is influenced by sea surface temperatures and changes in insolation (Burrough and Thomas, 2008).

Displacement along the northeast trending faults of the ORZ may have altered river flow directions (Shaw, 1988; Shaw et al., 2003). The southeast flowing rivers which include the proto-Okavango, Kwando and Zambezi were responsible for supplying the Kalahari sub-basins with lacustrine and deltaic sediment (Thomas and Shaw, 1992; Burrough et al., 2009b). The upper Zambezi and proto-Middle Zambezi rivers are

hypothesized to have combined and supplied water responsible for forming the mega-lakes. These rivers may also have combined with the Limpopo River or Orange River to supply water to the mega-lakes (Thomas and Shaw, 1992). The Zambezi contributed to basin inflow through back flooding events during significant increases of discharge (Burrough et al., 2009b).

The demise of mega-lakes is caused by periods of very low precipitation so that water is not being supplied to the lakes. Eventually the warm climate causes evaporation

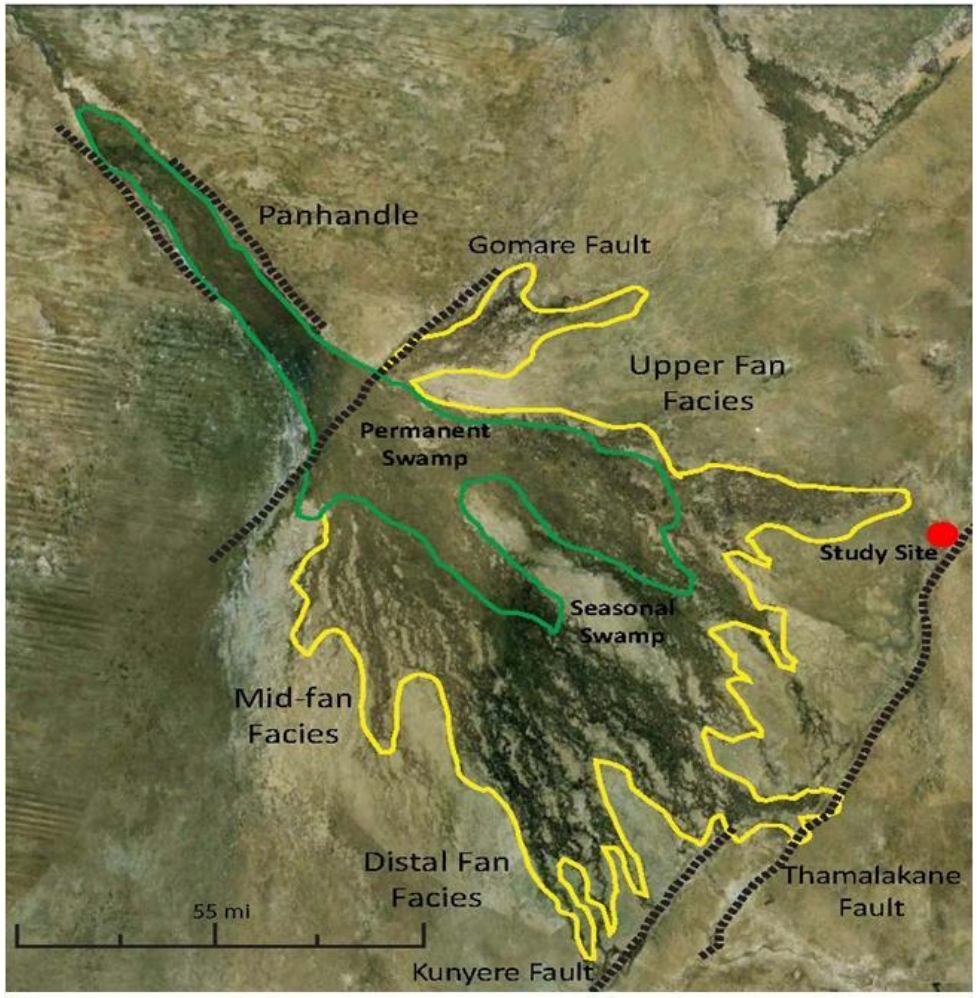

Fig. 3: The Okavango Delta and its sub-environments (modified from Google Earth).

of the lakes. In the past, rivers have diverted their paths due to tectonic events and changed the hydrology in the delta region (Haddon and McCarthy, 2005).

2.3 Sedimentation in the Okavango Delta

The Okavango Delta alluvial fan (Fig. 3) is formed within the ORZ, an extension of the East African Rift System (Stanistreet and McCarthy, 1993). Faulting along the Gomare fault to the northwest caused a change in the gradient of the Okavango River, initiating sedimentation to form an alluvial fan (McCarthy et al., 1997). The Okavango Delta can be divided into several regions: the Panhandle controlled by NW-trending faults, located at the apex of the fan where the Okavango River enters Botswana, a central region with perennial swamps where water is confined by vegetation, and seasonal swamps where water is comparatively unconfined (McCarthy et al., 1988). The Okavango Delta alluvial fan is classified as a low gradient, low sinuosity, highly vegetated fan system (Stanistreet and McCarthy, 1993). Unlike the typical alluvial fans in arid environments that are built by periodic discharge, the Okavango Delta alluvial fan was formed and modified by a permanent stream, the Okavango River and its distributaries. The distributary channels are initiated in the proximal portion of the alluvial fan within the permanent swamp (Stanistreet and McCarthy, 1993).

The upper fan facies are not characterized by braided or debris-flow deposits, typical of arid alluvial fans, but are dominated by meandering river systems (McCarthy et al., 1992). Fluvial sedimentation on the fan is restricted to the channels of the distributary systems in the permanent swamp (McCarthy and Ellery, 1995). The channel margins are confined by vegetated levees comprised mainly of peat, stabilized by living plant

communities dominated *by Cyperus papyrus* or *Phragmites Spp*, and are resistant to erosion (McCarthy et al., 1988; McCarthy et al., 1991). The strong influence of vegetation on the Okavango Delta alluvial fan differs greatly from other types of alluvial fans. The channel margins are permeable so that water from the channels leak through the levees creating swamp vegetation in the adjacent floodplains (Stanistreet and McCarthy, 1993). Therefore, water discharge decreases downriver and most of the bedload in the Okavango Delta alluvial fan is contained in the upper fan facies (McCarthy et al., 1991).

In the mid-fan region, stream channels infill, often become inactive and shift laterally (Nilsen, 1982). In the Okavango Delta, the mid-fan facies receives deposition from channel-bed aggradation within the distributaries. The distributary channels rapidly aggrade as velocity of discharge decreases (McCarthy et al., 1992). These channels become blocked and ultimately fail which causes avulsion. The channel is diverted to a lower elevation in the floodplain, creating a widespread distribution of primarily fine grained bedload sand on the alluvial fan (McCarthy et al., 1992). The failure of primary channels creates a need for secondary channels. These secondary channels remain stable as they are not blocked by swamp vegetation, and supply water to the distal portion of the fan (McCarthy et al., 1992).

The distributary channels of the upper and mid-fan facies contribute fluvial sediment to the distal portion of the delta. At the distal facies, bedload transported through the mid-fan region is deposited into small to large lake basins (McCarthy et al., 1991). After the formation of the Okavango Delta alluvial fan, the alluvial fan deposits are modified by fluvial processes associated with the distributary channels. The formation of lakes near the distal portion of the fan allows sedimentation by lacustrine processes.

During a wet climate, or times of high river discharge, the channels of the distributary system may produce splays forming a body of water, or lake at the distal end of an alluvial fan (Nichols and Fisher, 2007). The channels may then backfill with lacustrine deposits (Nichols and Fisher, 2007). When this happens, lacustrine and distal fluvial facies intermingle.

The depositional facies of a lake are affected by changes in biological, chemical and physical aspects of the environment. For mega-lakes which have been suggested to form in the Okavango region, terrigenous sediments in association with lacustrine sedimentation can develop from wind or wave action and river input (Davis, 1983). The clay and silt size sediments tend to occur in the middle, stable part of the lake, accumulating from suspension. The fine-sized grains are commonly distributed over wide areas, while coarser grain sediments occur on the outer edges of a lake (Davis, 1983).

A groundwater exploration program drilled 150 boreholes into the Kalahari Beds in the distal part of the Okavango Delta alluvial fan (Milzow et al., 2009). Gamma ray and resistivity measurements were recorded in boreholes to interpret the lithology. The sandstones were determined to be associated with fluvial deposition and clay and siltstones were associated with lacustrine deposition (Milzow et al., 2009). During wetter periods, lakes formed on the downthrown side of the Kunyere and Thamalakane faults (Milzow et al., 2009). When the climate dried, rivers dominated the area leading to fluvial deposition of sands. The interpretation of the depositional system identified alternating fluvial and lacustrine deposition in the distal portion of the Okavango Delta (Milzow et al., 2009).

The Okavango Delta alluvial fan is located in a semi-arid environment. Therefore the region has been affected by aeolian processes. During dry periods, sand is moved by wind (Ahlbrandt and Fryberger, 1982). Aeolian features such as linear dunes that exist around the delta contribute sand-sized grains to the distal portion of the fan (McCarthy and Ellery, 1995). Aeolian deposition is uniform over the fan because it does not depend on the distribution of water (Milzow et al., 2009).

The distal part of the Okavango Delta alluvial fan which terminates at the Thamalakane Fault. Therefore it is being influenced by fluvial processes from the distributary channels, lacustrine processes from lakes that form along the faults that bound the delta, and aeolian processes that occur during arid climate.

CHAPTER III

METHODOLOGY

3.1 Sediment Sampling

Sediments were retrieved from the wall of a quarry (Fig. 4) in the distal portion of the Okavango Delta (19º 16'46.14" S, 23º 55'33.62" E) in June 2010 and 2011 (Fig. 3). The samples were collected at 5 centimeter intervals from the surface to a depth of 6.5 m.

Fig. 4: Sediments being collected from the wall of a quarry (19º 16'46.14" S, 23º 55'33.62" E)

The sediments were stored in labeled plastic ziploc bags and transported to the laboratory for further analyses. In the laboratory, an aliquot of the sediment was dried at 60°C for 48 hours and then stored in clean plastic containers.

3.2 Sample Analyses

3.2.1 Color Description

A description of the color was made on the dried sediment from each sample interval using a Munsell color chart. The Munsell color number and description were recorded for each sampled interval.

3.2.2 Grain Size Analysis

Grain size distribution (% clay, silt and sand) was determined using a Cilas 1180 laser particle size analyzer. Approximately 15 g of dried sediment from each sampled interval was placed into 50 ml plastic centrifuge tubes. About 40 mL of 10% hydrochloric acid (HCl) was poured into the centrifuge tube and allowed to react overnight to digest carbonates. After digestion of the carbonates, the samples were centrifuged and the supernatant was decanted. After the initial decanting of the HCl, deionized water was added to each sample, mixed with a vortex mixer, and centrifuged to rinse the residual HCl from the samples. This step was repeated until the decanted liquid tested neutral on pH paper. The samples were then placed in a drying oven at 50º C for twenty four hours to dry. Next, organic matter in the sample was removed by hydrogen peroxide (H_2O_2) digestion. A 20 ml 30% H_2O_2 solution was mixed with the sediments and allowed to react overnight. The samples were centrifuged and the H_2O_2 in the samples was then decanted and rinsed four times with 40 mL of deionized water in the same process as before. The samples were kept in suspension using 25 mL of a 5.5 g/L sodium metaphosphate (NaO_3P), and the sediment solution was stirred using a magnetic stirrer. An aliquot of the sample was introduced into the laser particle size analyzer, and

the output from the laser particle size analyzer was used to determine the grain size distribution from statistics using the Folk and Ward (1957) method. The laser particle analyzer directly measures particles between 0.04 and 2,500 μm, and then transfers the micrometer measurement to grain size in phi (Ø). The graphic standard deviation (Friedman, 1967) was calculated using:

$$SDg= (Ø84-Ø16)/(4)+((Ø95-Ø5)/(6.6)$$

the graphic skewness was calculated using:

$$SKg=:(Ø84+Ø16-2Ø50))/(2(Ø84-Ø16))+ ((Ø95+Ø5-2Ø50))/(2(Ø95-Ø5)$$

and graphical mean was calculated using:

$$Mg= (Ø16+ Ø50+ Ø84)/3$$

Ø95 is the grain size at the 95th percentile, Ø84 at the 84th percentile, Ø16 at the 16th percentile, and Ø5 at the 5th percentile (Friedman, 1967).

3.2.3 Measurement of Dry Bulk Density

The dry bulk density was measured by gravimetric analysis. Sediment from each interval was filled into 10 cm^3 pre-weighed plastic cups. The mass of the sediments was determined gravimetrically and the dry bulk density was calculated by dividing the mass of sediment by the volume of the container.

3.2.4 Measurement of Magnetic Susceptibility

A Barrington magnetic susceptibility meter with an MS2B dual frequency sensor was used to determine the magnetic susceptibility. The sediment in the 10 cm^3 pre-

weighed plastic cups that were used for dry bulk density were re-used to measure magnetic susceptibility. The magnetic susceptibility meter was set to the high frequency mode and the mass of the sediment was used in the estimate of the magnetic susceptibility of the sediment.

3.2.5 Measurement of Biogenic Silica

The method of Mortlock and Froelich (1989) was used to determine biogenic silica. Approximately 25-200 mg of dry sediment was placed into 50 ml centrifuge tubes and reacted with 10% H_2O_2 to remove organic matter and then reacted with 1N HCl to digest carbonates. A 40 ml aliquot of 2M sodium carbonate ($Na_2CO_{3)}$ was added to each centrifuge tube and the samples were placed in a hot water bath at 85º C for 5 hours. After the 5 hours, the samples were centrifuged for 5 minutes at 5280 g. After centrifugation, about 30 mL of the supernatant was transferred to plastic containers with liner less lids. The amount of biogenic silica extracted was determined by a modified molybdate-blue spectrophotometry technique (Mortlock and Froelich, 1989). The silica calibration standards were prepared by dissolving variable amounts of sodium silicofluoride (Na_2SiF_6) in deionized water. The calibration standards used ranged from 0.005 µM to 0.123 µM and had a correlation coefficient of 0.9999. The weight percent of silica was calculated by using the equation: %SiOPAL= 112.4 X (Cs/M); where Cs is the silica concentration (µM) of the sample and M is the sample mass (mg) that was measured (Mortlock and Froelich, 1989).

3.2.6 Diatom Preparation

10 slides were prepared to assess the samples for presence of diatoms using guidelines by the University College of London Department of Geography (http://www.geog.ucl.ac.uk). The sample intervals used were: 5-10 cm, 80-85 cm, 170-175 cm, 235-240 cm, 275-280 cm, 330-335 cm, 465-470 cm, 540-545 cm, 565-570 cm, and 635-640 cm. To prepare the samples approximately 0.02 grams of dried sediment was placed into centrifuge tubes. Five mL of 30% H_2O_2 was added to each tube and placed into an 80°C hot water bath for 5 hours to remove organic matter. The samples were mixed every hour during the 5 hour immersion in the water bath. After 5 hours, 1-2 drops of 50% HCl was added to each sample to remove carbonates. The samples were left to settle out overnight. The supernatant liquid was decanted out and resuspended in distilled water. This process was repeated until organic matter was removed. Next, the diatoms were placed onto a slide with an eye dropper, and then left to dry overnight. Nafrax was added to each slide to enhance the diatoms for microscopic examination.

3.2.7. Measurement of Organic and Inorganic Carbon Concentrations

The total organic carbon (TOC) and total inorganic carbon (TIC) was measured by analyzing the carbon in the form of CO_2 by coulometric titration using a UIC CM5014 Coulometer after the method of White (1966). Before each analysis, at least two blanks were run followed by at least two $CaCO_3$ standards for calibration. The standards gave a precision of no greater than 0.5% for both total carbon and total inorganic carbon measurements. For total carbon, about 30 mg of sediment was placed into a porcelain boat and loaded into the furnace at 950º C which allows the direct measurement of total

carbon as $CO_{2(g)}$ liberated from the combustion in a furnace. For total inorganic carbon, about 100 mg of sediment was weighed into a Teflon boat and then placed in a glass reaction tube. The CM5014 Coulometer allows direct measurement of total inorganic carbon by acidification using perchloric acid ($HClO_4$). The released CO_2 was calculated by coulometric titration. Total organic carbon is determined by the difference between total carbon and total inorganic carbon.

3.2.8 Measurement of Stable Isotopes of Inorganic Carbon and Oxygen

The stable carbon isotope and the stable oxygen isotope of inorganic $\delta^{13}C$ and $\delta^{18}O$ was determined by acidification under a vacuum and extracting the $CO_{2\ (g)}$ on a vacuum line using the technique of Krishnamurthy et al. (1997). The $CO_{2\ (g)}$ was sealed in Pyrex tubes and later introduced into the Thermo Finnigan Deltaplus XL mass spectrometer to determine the $\delta^{13}C$ and for $\delta^{18}O$ of the $CO_{2\ (g).}$ The $\delta^{13}C$ values are reported in per mill (‰) relative to VPDB international standard and the $\delta^{18}O$ values are reported in per mill (‰) relative to VSMOW international standard. The routine measurements of house standards gave an overall precision better than 0.1 ‰ for both $\delta^{13}C$ and $\delta^{18}O$ measurements.

CHAPTER IV

RESULTS

4.1 Physical Properties of sediments

The results for Munsell Color and Number, percent clay, silt and sand, moment mean, moment standard deviation, moment skewness, graphic mean, graphic standard deviation, graphic skewness, magnetic susceptibility, TIC, total carbon, TOC, $\delta^{13}C_{TIC}$, $\delta^{18}O_{TIC}$, dry bulk density, and biogenic silica are tabulated and presented in Appendices 1 to 3.

4.2 Lithology

The lithologic section is divided into 8 units. This is based on vertical variations in magnetic susceptibility, dry bulk density, percent clay, silt and sand, total inorganic and organic carbon and biogenic silica (Fig. 5 and 6). The color bar for the different depths shows the Munsell Color of the sediments. Unit I occurs from the surface to 60 cm and Unit II is from 60 to 125 cm. The depth interval for Unit III is from 125 cm to 195 cm. Unit IV ranges in depth from 195 cm to 325 cm and Unit V ranges from 325 cm to 420 cm. The depth for Unit VI ranges from 420 cm to 525 cm, Unit VII ranges from 525 cm to 625 cm and finally, the basal unit representing Unit VIII occurs from 625 cm to the maximum depth at 650 cm.

4.2.1 Unit I (0-60 cm)

The Munsell color is very dark grayish brown (10YR 3/2) from the surface to 20 cm and lightens to a dark grayish brown (10YR 4/2) color from 25 cm to the bottom of the unit. There is a continuous decrease in magnetic susceptibility from 6 E -08 m^3/kg at the surface to 5 E -08 m^3/kg to the bottom of the unit (Fig. 5). The dry bulk density values remain constant throughout the unit with values averaging 1.66 ± 0.028 g/cm^3 (Fig. 5). The clay fraction ranges from 2.4% to 10%, the silt fraction from 10% to 35%, and the sand fraction from 55% to 88% (Fig. 5). Clay and silt fractions show a slight increase from the surface to 15 cm, followed by a slight decrease to 55 cm. There is another increase from 55 cm to 60 cm. The sand fraction in this unit displays depth variations opposite to that of the clay and silt fractions. The sand fraction at the top of the unit begins with a slight decrease to 15 cm followed by an increase to 55 cm. There is a slight decrease from 55 cm to the bottom of the unit (Fig. 5). The sorting determined from graphic standard deviation ranges from 1.19 to 2.13. Sorting increases from the surface to 15 cm, followed by a decrease to 60 cm (Fig. 5).

The total inorganic carbon (TIC) remains at values that average 0.0265 ± 0.015% (Fig. 6). There are only a few $\delta^{13}C_{TIC}$ and $\delta^{18}O_{TIC}$ values in unit I due to nearly 0% TIC concentrations in the sediment. The $\delta^{13}C_{TIC}$ generally increase from -9.2‰ at the surface to -8.3‰ at 35 cm (Fig. 6). The $\delta^{18}O_{TIC}$ isotope values slightly increase from 23.0‰ to 25.0‰ from the surface to 35 cm (Fig. 6). The total organic carbon (TOC) increases from 0.67% at the surface to 0.93% at 5 cm. The TOC concentration then decreases to 0.46 % at 60 cm (Fig. 6). Biogenic silica in this unit ranges from 0.023 µM at the surface to

0.073 µM at the bottom of the unit, and increases continuously from the top of the unit to the bottom of the unit (Fig. 6).

4.2.2 Unit II (60-125 cm)

The Munsell color is dark grayish brown (10YR 4/2) color from 60 cm to the bottom of the unit. There is a continuous decrease in magnetic susceptibility from 5 E -08 m^3/kg at the surface to 4 E -08 m^3/kg to the bottom of the unit (Fig. 5). The dry bulk density values remain constant throughout the unit with values averaging 1.66 ± 0.039 g/cm^3 (Fig. 5). The clay fraction ranges from 5.5% to 19%, the silt fraction from 17% to 57%, and the sand fraction from 23% to 77% (Fig 5). Clay and silt fractions show a decrease to the bottom of the unit. The sand fraction in this unit displays depth variations opposite to that of the clay and silt fractions. The sand fraction shows a slight decrease from 60 cm to 75 cm that is followed by an increase to the bottom of the unit (Fig. 5). The sorting ranges from 1.42 to 2.24. The sorting increases from 60 cm to 70 cm and then remains relatively constant averaging 2.13 ± 0.083 to the bottom of the unit (Fig. 5).

The TIC concentration remains at values that average 0.027 ± 0.015% (Fig. 6). The $\delta^{13}C_{TIC}$ generally increase from -7.7‰ to -6.5‰ from 90 cm to 100 cm followed by a decrease to -7.5‰ from 100 cm to 125 cm (Fig. 6). The $\delta^{18}O_{TIC}$ show a slight decrease 24.4‰ at 90 cm to 23.7‰ to 125 cm (Fig. 6). The TOC concentration generally increases from 0.11% at 60 cm to 0.45% at 125 cm (Fig. 6). Biogenic silica in this unit ranges from 0.07 µM at 60 cm to 0.097 µM at the bottom of the unit, and increases continuously from the top of the unit to the bottom of the unit (Fig. 6).

4.2.3 Unit III (125-195 cm)

The Munsell colors from 125 cm to 140 cm are grayish brown (10YR 5/2) colors transitioning into a light brownish gray (10YR 6/2) color at 145 cm to 190 cm. At 195 cm the Munsell color is pale brown (10YR 6/3). The magnetic susceptibility decreases continuously from 5 E -08 m^3/kg at 125 cm to 2 E -08 m^3/kg to the bottom of the unit (Fig. 5). The dry bulk density decreases from 1.69 g/cm^3 at 125 cm to 1.52 g/cm^3 at 165 cm. It then increases to 1.63 g/cm^3 at 170 cm, remaining constant to the bottom of the unit (Fig. 5). Sediment grain size in this unit is variable. The clay fraction is nearly constant from 125 cm to 185 cm with relatively low frequency fluctuations from 4.4% to 7.6%. There is a decrease from 190 cm to 195 cm to 2.4% (Fig. 5). The silt fraction increases from 17% at 125 cm to 59% at 180 cm. The silt fraction then decreases to 17.5% at 195 cm (Fig. 5). The sand fraction begins with a decrease from 77% at 125 cm to 33% at 180 cm. There is an increase to 80% at 195 cm (Fig. 5). The sorting decreases from 1.98 at 125 cm to 1.39 at 145 cm. There is a sharp increase to 2.09 at 155 cm, followed by a decrease to 1.39 to the bottom of the unit (Fig. 5).

The TIC concentration increases from 0.07% at 125 cm to 0.84% at 155 cm. The TIC concentration remains nearly constant at an average of 0.76 ± 0.07% from 155 cm to 195 cm (Fig. 6). The $\delta^{13}C_{TIC}$ increases from -7.5‰ at 125 cm to -6.6‰ at 195 cm (Fig. 6). The $\delta^{18}O_{TIC}$ has a very low frequency fluctuation between 21.6‰ and 23.6‰ from 125 cm to the bottom of the unit (Fig. 6). The TOC concentration ranges from 0.69% to 0.31% decreasing continuously from 125 cm to the bottom of the unit (Fig. 6). Biogenic silica concentration generally increases from 0.087 µM at 125 cm to 0.109 µM at 185 cm followed by a decrease to 0.026 µM at 195 cm (Fig. 6).

4.2.4 Unit IV (195-325 cm)

The Munsell color is pale brown (10YR 6/3) at 195 cm to 200 cm and transitions to very pale brown (10YR 7/3) at 205 cm. The sediment interval between 205 cm to 265 cm lightens to a very pale brown (10YR 8/2) Munsell color. The Munsell color darkens to very pale brown (10YR 7/4) from 265 cm to 325 cm. The magnetic susceptibility increases from 2 E -08 m^3/kg at 195 cm to 5 E -08 m^3/kg at 325 cm (Fig. 5). The dry bulk density remains nearly constant averaging 1.56 ± 0.027 g/cm^3 from 195 cm to 270 cm. The dry bulk density decreases and averages 1.39 ± 0.027 g/cm^3 from 270 cm to 325 cm (Fig. 5). The clay fraction has low frequency fluctuations from 2.4% to 6.7% from 195 cm to the bottom of the unit (Fig. 5). The silt fraction fluctuates from 14% and 40% from 195 cm to the bottom of the unit, with a slight increase towards the base (Fig. 5). The sand fraction fluctuates between 56% and 80% from 195 cm to the bottom of the unit, with a slight decrease towards the base (Fig. 5). The sorting fluctuates between 1.32 and 2.04 from 195 cm to 295 cm. At 300 cm it remains relatively constant averaging 1.82 ± 0.024 to 320 cm. There is a decrease in sorting to 1.52 at the bottom of the unit (Fig. 5).

The TIC concentration has a marked increase from 0.07% at 125 cm to 2.49% at 260 cm. This is followed by a continuous decrease to 0.14% at 325 cm (Fig. 6). The $\delta^{13}C_{TIC}$ shows a marked increase from -6.6‰ at 195 cm to -3.6‰ at 260 cm, followed by a general decrease to -7.0‰ at 315 cm. The $\delta^{13}C_{TIC}$ increases to -5.4‰ at 325 cm (Fig. 6). The $\delta^{18}O_{TIC}$ fluctuates between 22.0‰ and 28.3‰ from 195 cm to the bottom of the unit (Fig. 6). The TOC concentrations decrease from 0.31% at 195 cm to 0.07% at 230 cm, and then there is a marked increase to 0.45% at 290 cm, followed by a continuous decrease to 0.21% to the bottom of the unit (Fig. 6). Biogenic silica concentration

increases from 0.026 µM at 125 cm to 0.108 µM at 210 cm. Biogenic silica concentration generally increases with fluctuations between 0.026 µM and 0.133 µM between 215 cm and 305 cm. There is a marked decrease to 0.048 µM at 325 cm (Fig. 6).

4.2.5 Unit V (325-420 cm)

The Munsell color is very pale brown (10YR 7/4) from 325 cm to 365 cm, then transitions to very pale brown (10YR 7/3) at 365 cm to 385 cm. The sediment interval between 385 cm and 410 cm lightens to very pale brown (10YR 8/2). The Munsell color starts to get darker, transitioning to very pale brown (10YR 7/3) from 415 cm to 420 cm. The magnetic susceptibility has an overall decrease from 5 E -08 m^3/kg at 325 cm to 4 E -08 m^3/kg at 415 cm, with a marked increases at 420 cm (8 E -08 m^3/kg) (Fig. 5). The dry bulk density fluctuates between 1.16 g/cm^3 and 1.56 g/cm^3 from 325 cm to the bottom of the unit (Fig. 5). The clay fraction fluctuates between 3.1% and 7.7% from 325 cm to the bottom of the unit (Fig. 5). The silt fraction shows higher frequency fluctuations between 16% and 54% from 325 cm to the bottom of the unit (Fig. 5). The sand fraction also shows high frequency fluctuations between 56% and 88% from 325 cm to the bottom of the unit (Fig. 5). The sorting shows fluctuations between 1.31 and 2.03 from 325 cm to the bottom of the unit (Fig. 5).

The TIC concentration remains mostly at background values of 0.2% with a slight increase at 420 cm (0.44%) (Fig. 6). The $\delta^{13}C_{TIC}$ fluctuate between -4.5‰ and -8.8‰, and the $\delta^{18}O_{TIC}$ fluctuate between 26.2‰ and 35.1‰ throughout the unit (Fig. 6). The TOC concentration decreases from 0.25% at 330 cm to 0.16% at 395 cm. TOC

concentrations then increase from 0.16% at 395 cm to 0.4% at 400 cm, and remains nearly constant averaging 0.40 ± 0.0036% to 415 cm. There is a slight increase to 0.52% at 420 cm (Fig. 6). The biogenic silica concentration is 0.048 µM at 325cm and then has a general decrease from 0.107 µM at 330 cm to 0.071 µM at 400 cm. There is a marked increase to 0.164 µM at 360 cm, and a slight increase to 0.11 µM from 400 cm to 420 cm (Fig. 6).

4.2.6 Unit VI (420-525 cm)

The Munsell color from 420 cm to 425 cm is very pale brown (10YR 7/3), then light to brownish gray (10YR 6/2) between 430 cm and 435 cm. The Munsell color alternates between very pale brown (10YR 7/3) and very pale brown (10YR 8/2) from 440 cm to 525 cm. The magnetic susceptibility begins with a marked increase at 420 cm (8 E -08 m^3/kg), but has an overall decrease from 5 E -08 m^3/kg at 425 cm to 2 E -08 m^3/kg at 525 cm, interrupted with an increase at 470 cm (6 E -08 m^3/kg) (Fig. 5). The dry bulk density fluctuates between 1.16 g/cm^3 and 1.54 g/cm^3 from 420 cm to the bottom of the unit. This unit shows the most fluctuation in the dry bulk density (Fig. 5). The clay fraction fluctuates between 1.9% and 7.7% from 420 cm to the bottom of the unit (Fig. 5). The silt fraction shows higher frequency fluctuations between 9% and 54% from 420 cm to the bottom of the unit (Fig. 5). The sand fraction also shows high frequency fluctuations between 38% and 88% from 420 cm to the bottom of the unit (Fig. 5). The sorting shows high frequency fluctuations as well that range from 1.04 to 1.98 to the bottom of the unit (Fig. 5).

The TIC concentration remains mostly at background values of 0.2% with slight increases at 420 cm (0.44%) and 470 cm (0.31%) (Fig. 6). The $\delta^{13}C_{TIC}$ shows high frequency fluctuations between -5.5‰ and -8.0‰, and the $\delta^{18}O_{TIC}$ also show high frequency fluctuations between 19.1‰ and 34.4‰ from 420 cm to 525 cm (Fig. 6). The TOC concentration is 0.52% at 420 cm, and decreases to an average of 0.40 ± 0.029%, remaining relatively constant from 425 cm to 500 cm. TOC then decreases to 0.10% from 500 cm to 525 cm (Fig. 6). The biogenic silica concentration has a general decrease from 0.11 µM at 420 cm to 0.03 µM at 500 cm. There is a marked increase to 0.108 µM at 480 cm. The biogenic silica concentration increases from 0.077 µM at 485 cm to 0.105 µM at 525 cm (Fig. 6).

4.2.7 Unit VII (525-625 cm)

The Munsell color at 525 cm is very pale brown (10YR 7/3). From 525 cm to 610 cm the Munsell color is white (10YR 8/1), and then transitions to very pale brown (10YR 8/2) to the bottom of the unit. The magnetic susceptibility remains nearly constant averaging 1 E -08 ± 4.0 E-09 m^3/kg from 525 cm to 625 cm (Fig. 5). The dry bulk density remains nearly constant averaging 1.41 ± 0.09 g/cm^3 from 525 cm to 625 cm (Fig. 5). The clay fraction decreases from 3.4% at 525 cm to 1.7% at 530 cm and then remains nearly constant, averaging 1.5 ± 0.33% from 530 cm to the bottom of the unit (Fig. 5). The silt fraction decreases from 23% at 525 cm to 4% at 550 cm and then remains nearly constant, averaging 4 ± 1.21 % (Fig. 5). The sand fraction increases from 74% at 525 cm to 94% at 550 cm and then remains nearly constant, averaging 95 ± 1.5% from 550 cm to the bottom of the unit (Fig. 5). The sorting decreases from 1.42 at 525 cm

to 0.56 at 560 cm and then remains nearly constant averaging 0.61 ± 0.109 to the bottom of the unit (Fig. 5).

The TIC concentration remains nearly constant at background values averaging 0.19 ± 0.02% from 525 cm to 625 cm (Fig. 6). The $\delta^{13}C_{TIC}$ fluctuate between -5.5‰ to -8.0‰, and the $\delta^{18}O_{TIC}$ fluctuate between 19.1‰ and 27.4‰ from 525 cm to the bottom of the unit (Fig. 6). The TOC concentration remains nearly constant at 0.09% from 525 cm to 560 cm with a marked increase to 0.26% at 545 cm. The TOC concentration increases to values averaging 0.29 ± 0.05% that remains nearly constant from 550 cm to the bottom of the unit (Fig. 6). Biogenic silica concentration decreases from 0.105 µM at 525 cm to values that average 0.029 ± 0.01 µM from 530 cm to the bottom of the unit (Fig. 6).

4.2.8 Unit VIII (625-650 cm)

There is a dramatic change in the measured parameters that persist to the base of the stratigraphic section. The Munsell color is very pale brown (10YR 8/2) at 625 cm, then changes to dark grayish brown (10YR 4/2) from 630 cm to 635 cm and grayish brown (10YR 5/2) to 640 cm. The Munsell color transitions to a very pale brown (10YR 8/2) color to the base of the section. There is a marked increase in magnetic susceptibility at 630 cm where the values reach 7 E -08 m^3/kg. This is immediately followed by a marked decrease to 1 E -08 m^3/kg at the base of the unit (Fig. 5). The dry bulk density has a marked decrease at 630 cm to 0.93 g/cm^3 followed by an increase to 1.38 g/cm^3 to the base of the section (Fig. 5). The clay fraction increases from 2% at 625 cm to 15% at 635 cm. The clay fraction decreases to 1.7% at the base of the section (Fig. 5). The silt fraction follows a similar behavior as the clay fraction with a marked increase from 8% at

325 cm to 65% at 635 cm. This is also followed by a decrease to 6.6% to the bottom of the unit (Fig. 5). There is a marked decrease in the sand fraction from 90% at 625 cm to 21% at 635 cm, followed by an increase to 92% at 650 cm. As sand fraction decreases, there is an increase in silt and clay fractions (Fig. 5). The sorting increases from 0.95 at

625 cm to 2.22 at 635 cm. This is followed by a sharp decrease to 0.77 to the bottom of the unit (Fig. 5).

At 630 cm, there is also a slight increase in the TIC concentration. TIC concentrations spike from 0.18% at 625 cm to 0.45% at 630 cm. This is followed by a decrease in values to 0.22% to the base of the unit (Fig. 6). The $\delta^{13}C_{TIC}$ fluctuate between -5.7‰ and -6.6‰, and $\delta^{18}O_{TIC}$ fluctuate between 22.8‰ and 24.9‰ from 625 cm to the base of the section (Fig. 6). TOC concentrations remain constant through the unit, averaging values of 0.29 ± 0.04% (Fig. 6). Biogenic silica has a marked increase to 0.258 µM at 640 cm, then decreases to 0.065 µM from 645 cm to the base of the section (Fig. 6).

Table 1. Mean grain size ranges for all units.

Range	Unit 1	Unit 2	Unit 3	Unit 4	Unit 5	Unit 6	Unit 7	Unit 8
n =	12	13	14	26	19	21	20	5
% Sand	55-88%	23-77%	33-82%	56-84%	38-81%	42-89%	82-96%	21-92%
% Silt	10-35%	17-57%	16-60%	14-41%	16-54%	9-52%	1-2.5%	7-65%
% Clay	2-10%	5-19%	2-7.5%	3-7%	3-8%	2-6%	3-16%	2-15%

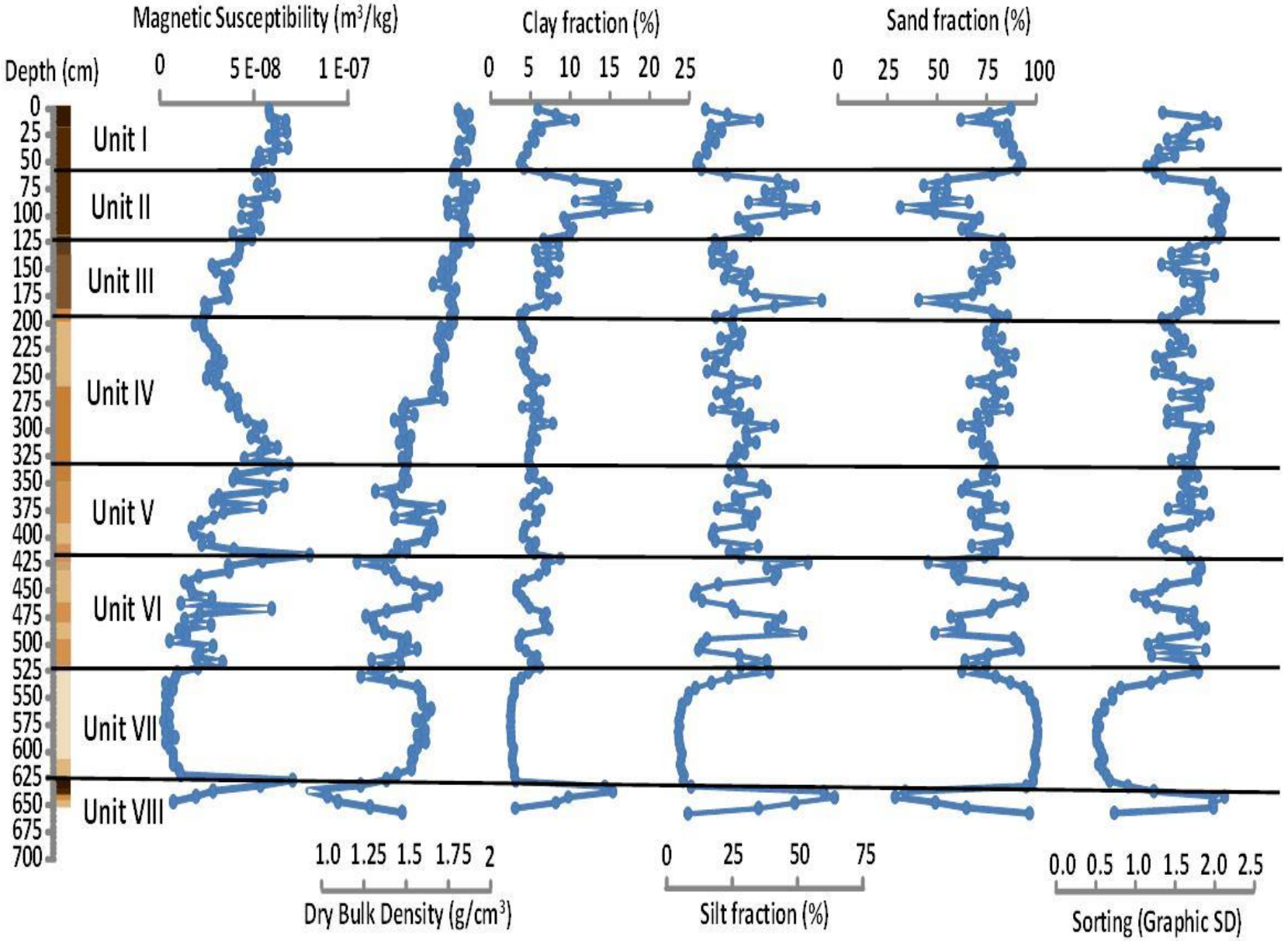

Fig. 5: Physical parameters: magnetic susceptibility, dry bulk density, percent clay, silt and sand, and sorting (graphic standard deviation).

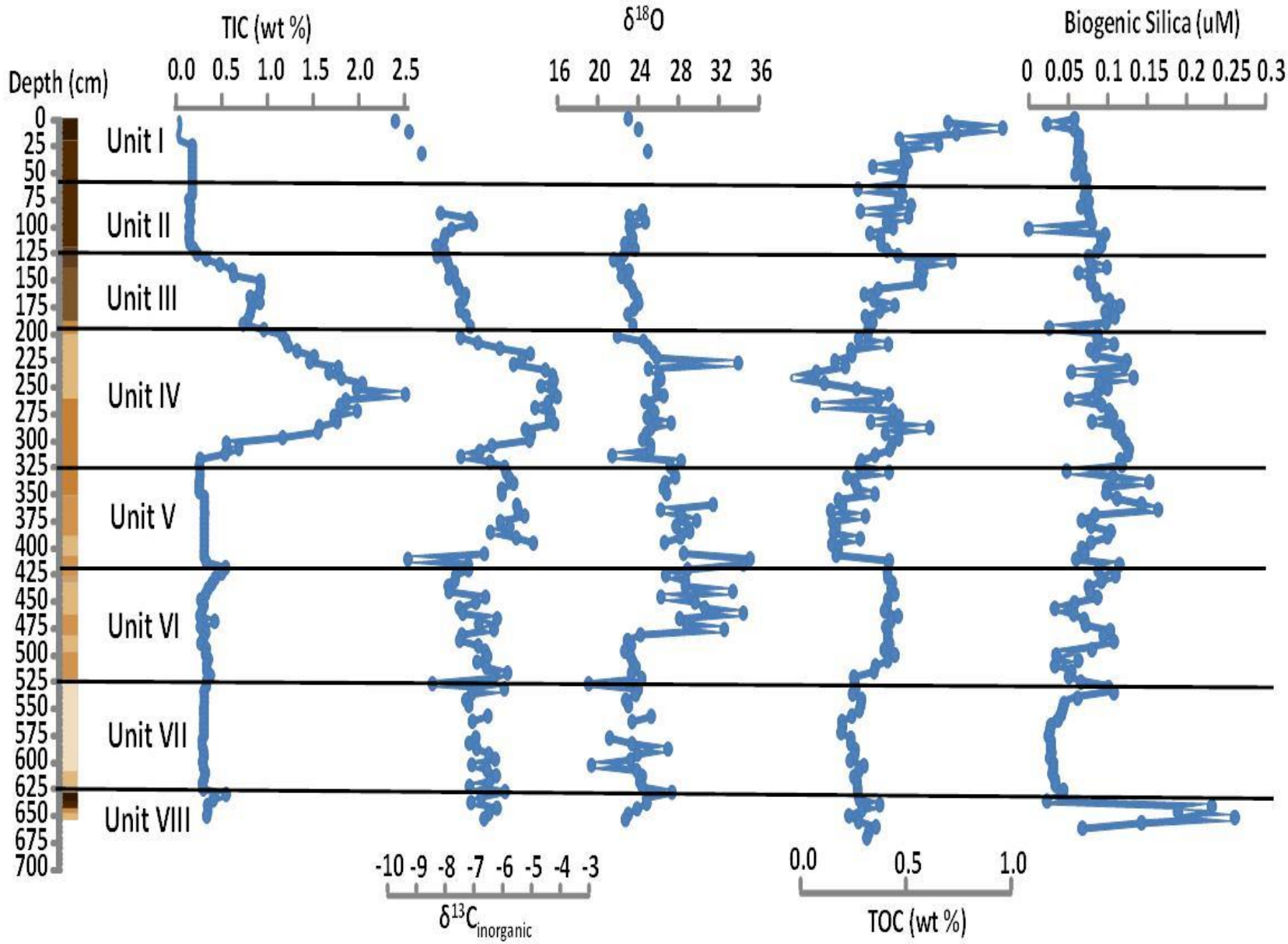

Fig. 6: Geochemical parameters: Total inorganic carbon (TIC), $\delta^{13}C$ of total inorganic carbon, $\delta^{18}O$, Total organic carbon (TOC) and biogenic silica.

CHAPTER V

DISCUSSION

5.1 Assessing Stratigraphy from the study site

Sedimentation at the distal end of the Okavango Delta alluvial fan where the study site is located is influenced by several types of depositional processes (Fig. 3). Fluvial, lacustrine and aeolian mechanisms work together to influence the sedimentation that is preserved in the sedimentary record (Fig. 5). Features such as pans and beach ridges are influenced by lake processes, and can indicate lacustrine formation. The term 'beach ridge', applies to stabilized, relict, aeolian or wave-built shore ridges that may consist of either siliclastic or calcareous clastic matter. Beach ridges can be used to reconstruct lake levels from vertical ridge sequences (Otvos, 2000). A pan, as used below, is a small, closed basin characteristic of arid and semi-arid environments of low relief that contain ephemeral lakes. Pan sediments are controlled by deposition of aeolian sediments in the shallow water and precipitation of evaporites (Holmgren and Shaw, 1997).

The Okavango sediments are sourced from ultra-mafic and felsic rocks derived from Angola (Huntsman-Mapila et al., 2005). The two major sources of sediment in the Okavango Delta alluvial fan are the wind-blown Kalahari sands and very fine-grained sand transported as bedload by the Okavango River (McCarthy and Ellery, 1998).

Different types of sediments from known depositional environments can be used to interpret depositional environments from the study site based on statistical parameters of grain size such as sorting and skewness (Friedman, 1967). There is a significant variation in the percent sand, silt and clay at the study site (Fig. 4). This suggests that more than one process may be responsible for sediment deposition at the study site.

5.2 Grain size Statistical data to Assess the stratigraphy

Bivariate plots of the graphical standard deviation (sorting) vs. graphic skewness (Fig. 7), graphical mean (Ø) vs. graphic skewness (Fig. 8), and clay + silt percentage vs. graphic skewness (Fig. 9) for the different stratigraphic units at the study site were used to assess aeolian, river and lake origins of sediments (Friedman, 1967). Tables 2 and 3 are presented to relate graphic mean, graphic skewness and sorting in terms of sediment characteristics (Folk, 1974). The statistical parameters at the study site are compared to Thomas (1987) and Friedman's (1967) graphic skewness, graphic mean, and sorting of sediments from known environments. On the plot of the graphic standard deviation vs. graphic skewness (Fig. 7) Friedman's line distinguishes between characteristics of beach and river sands, and is plotted as a dashed line. Although almost all the units from the study site lie on the river side of the line, it is still clear that the samples from unit VII are moderately well sorted, indicative of wind-blown sand. The other units show evidence of being a mixture of sediment from different sedimentary environments.

Table 2. Sorting and skewness parameters in terms of sediment characteristics.

Sorting Term	*Interval*	*Graphic Skewness*	*Interval*
Very well sorted	<0.35	Strongly fine-skewed	> +0.30
Well sorted	0.35-0.50	Fine skewed	+0.30 to +0.10
Moderately well sorted	0.5-0.8	Near symmetrical	+0.10 to -0.10
Moderately sorted	0.80-1.40	Coarse-skewed	-0.10 to -0.30
Poorly sorted	1.40-2.00	Strongly coarse-skewed	< -.30
Very poorly sorted	2.00-2.60		
Extremely poorly sorted	>2.6		

Table 3. Graphic Mean in terms of sediment characteristics.

Grain Size	*Graphic mean (Ø)*
Boulder	-12 to -8
Cobble	-8 to -6
Pebble	-6 to -2
Granular	-2 to -1
Very coarse grained	-1 to 0
Coarse grained	0 to 1
Medium grained	1 to 2
Fine grained	2 to 3
Very fine grained	3 to 4
Silt	4 to 8
Clay	<8

Forty six known beach ridge sediments and 21 known pan sediments were collected across the Kalahari by Thomas (1987). Grain size, graphic standard deviation, graphic skewness, and graphical mean (Ø) of the samples that were measured is displayed on bivariate plots to distinguish between beach and lacustrine depositional environments statistically (Thomas, 1987). Graphical mean (Ø) vs. graphic skewness and clay and silt percentage vs. graphic skewness are plotted for the beach ridges and pan sediments in Figures 8 and 9. Two large ovals presented in the figures represent the region in the plots occupied by beach ridge and pan sediments from beach ridge and pan sediments from Thomas (1987).

In Figure 8, the graphic mean increases from approximately 2.5 Ø to approximately 4 Ø, while the graphic skewness decreases from 0.2 to 0. From this point, the graphic mean then increases to 6 Ø and the graphic skewness increases to about 0.8. A similar distribution is observed in the clay and silt percentage vs. graphic skewness (Fig. 9), where the clay and silt percentages increases while the graphic skewness decreases, and then reverses with both increase in the clay and silt percentage and the graphic skewness. The stratigraphic units from the study site do not overlap in the region of pan sediments, indicating that this environment was not preserved or occurred in the stratigraphic section.

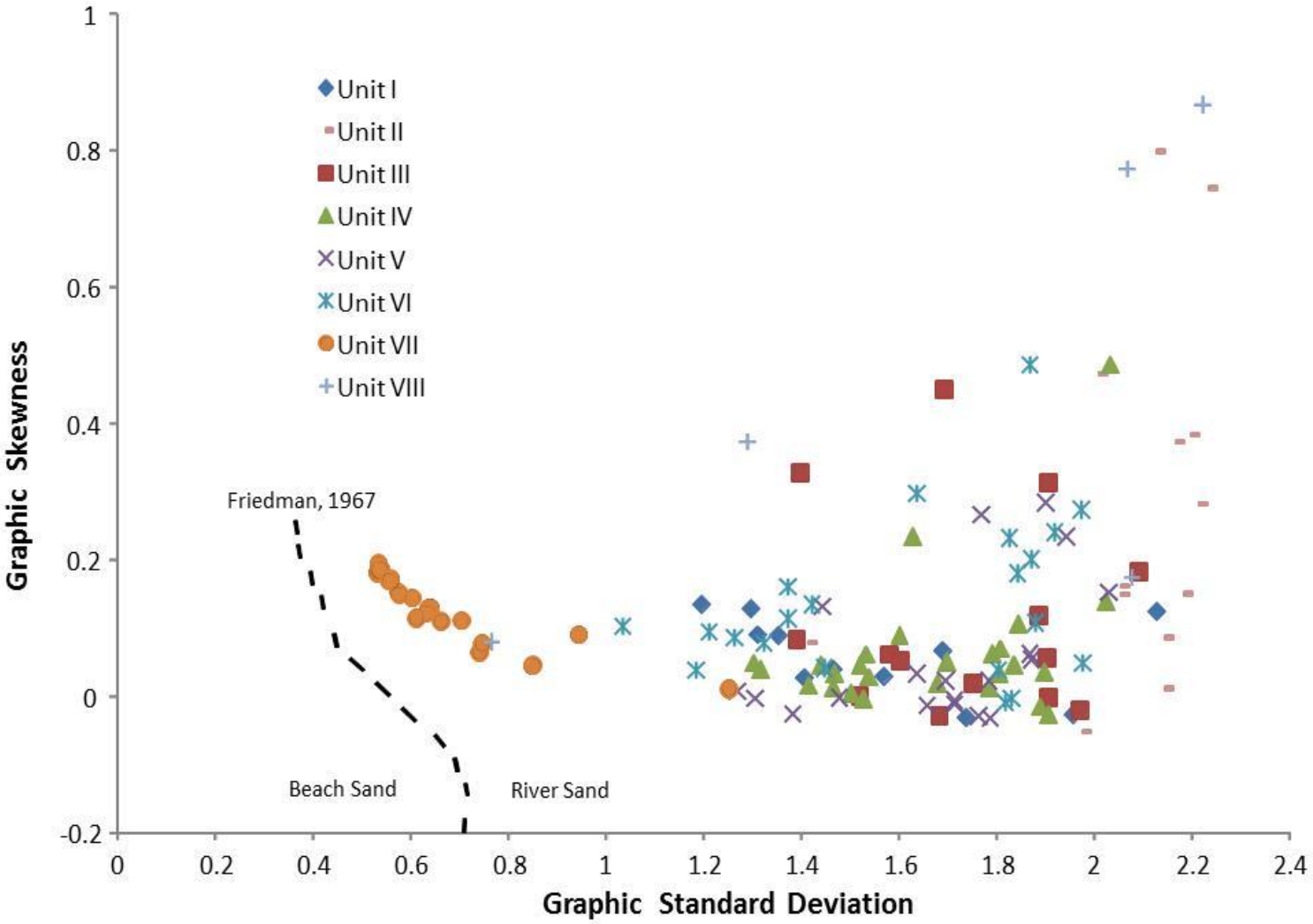

Fig. 7: Bivariate plot of graphic skewness and sorting (graphic standard deviation).

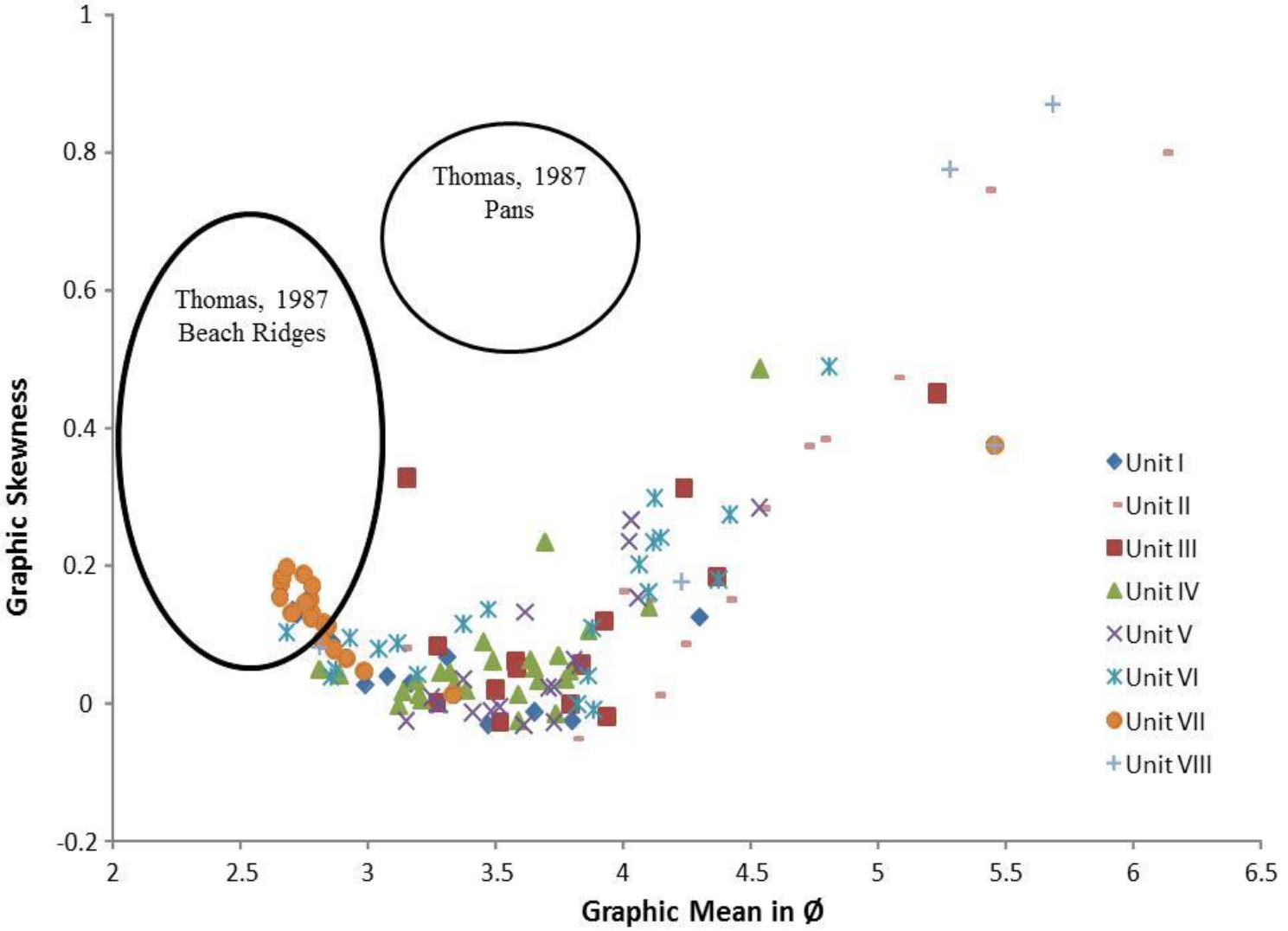

Fig. 8: Bivariate plot of graphic skewness and Graphic Mean.

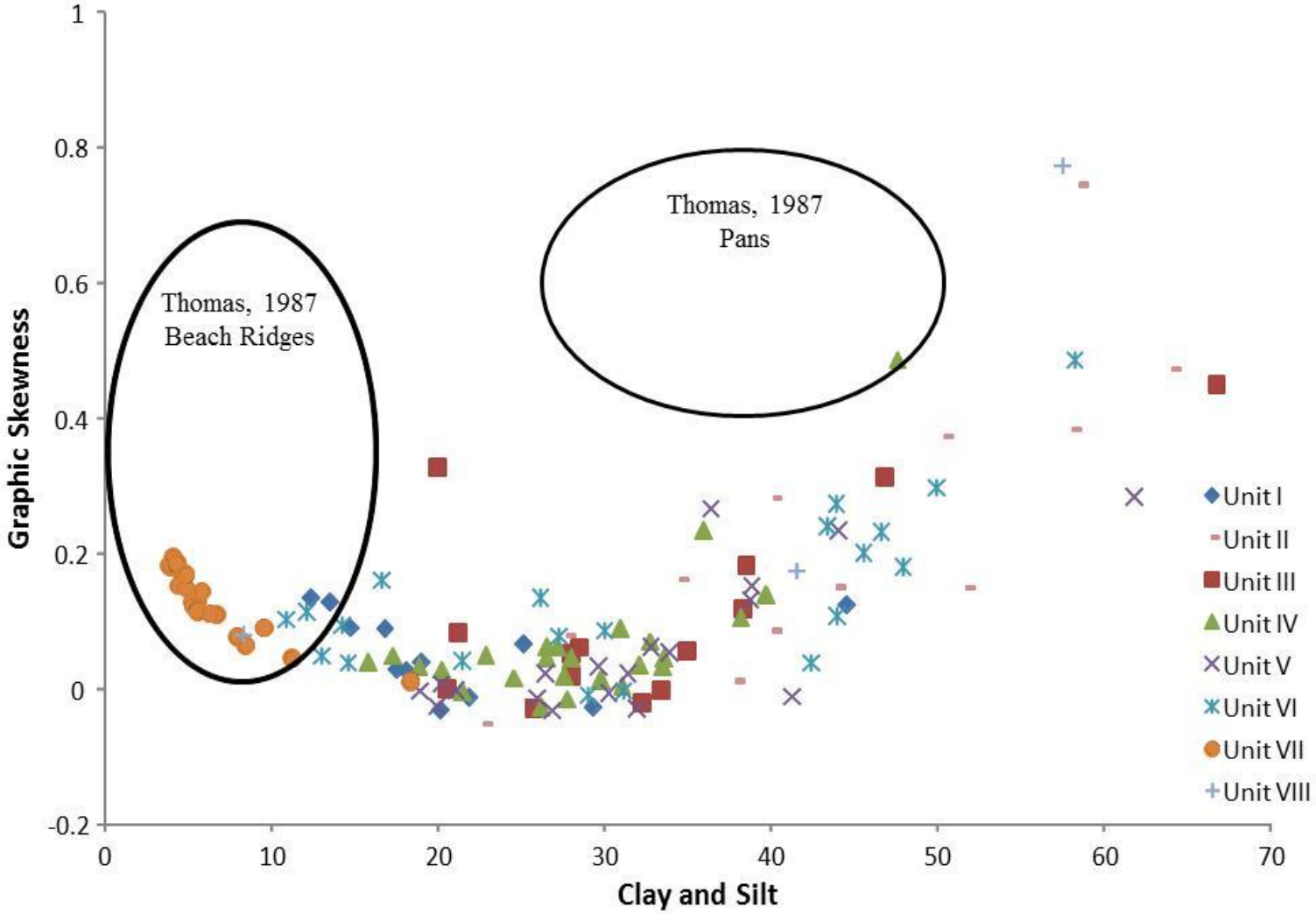

Fig. 9: Bivariate plot of graphic skewness and clay and silt fraction.

Although a textural analysis of sands in the Kalahari suggest that they are dominated by aeolian processes (Thomas, 1987), non-aeolian processes can rework the wind-sorted sand and leave little evidence that can be used to discriminate the reworking processes based on textural analysis (Thomas, 1987). It is evident that unit VII represents sediments with similar characteristics to those of wind-blown sediments since they are moderately well-sorted, and is likely derived from local dunes. The distribution of the data in Figures 8 and 9 suggest that an increase in graphic mean (Fig. 8) is due to an increase in silt and clay (Fig. 9). We suggest that the decrease in graphic skewness when graphic mean and clay and silt is increasing, represents a mixing of silt and clay (derived from a distal source) with the local sands from the Kalahari and therefore is attributed to fluvial transport during wet periods. On the other hand, when both the graphic mean and graphic skewness increase, then it is hypothesized that both the sand and clays are derived from the upper watershed of the Okavango River in subtropical Angola. This signifies a regional wet climate and supports the hypothesis that a mega-lake formed at the study site and is recorded in the stratigraphic section.

5.3 Variations in TIC Concentrations and the $\delta^{13}C_{TIC}$

The utility of carbonate minerals in understanding the process of deposition results from differences in concentrations and the variations in the stable carbon isotopic ratio ($\delta^{13}C_{TIC}$) within the stratigraphic units. Changes in the concentrations of carbonates can be related to variations in the supply to the sedimentary basin or from *in-situ* production of carbonates that precipitate from solution (Dean and Fouch, 1983). Variations in the $\delta^{13}C_{TIC}$ can be related to differences in the sources of TIC supplied from

the watershed to the sedimentary basin or to isotopic fractionation during precipitation of the carbonates formed from aqueous solution (Emrich et al., 1970).

Inorganic carbon in the Kalahari exists as calcium carbonate cemented duricrusts, known as calcrete (Nash and McLaren, 2003), and as sodium carbonates that exist on small islands in the Okavango Delta (McCarthy et al., 1998). Calcrete formed in the Kalahari can have a non-pedogenic or pedogenic origin (Ringrose et al., 1999; Nash and McLaren, 2003). Non-pedogenic calcrete originates from groundwater where carbonate is precipitated in the capillary fringe (Ringrose et al., 1999) due to high water table. Pedogenic calcrete on the other hand precipitates within the soil profile from evaporation of soil water (Ringrose et al., 1999). Climate directly affects the development of pedogenic and non-pedogenic calcrete. Calcretes preserved in lakes, pans and valleys in the Kalahari have both pedogenic and non-pedogenic origin (Nash and McClaren, 2003). Freshwater carbonates on islands and sediments in the Okavango Delta precipitate as trona (sodium carbonate) from evaporative enrichment in the dry season (McCarthy et al., 1998; Ringrose et al., 2009).

The vertical distribution of TIC concentrations from the study site shows concentrations up to 2.5% compared to the background values of 0.2% in unit III and unit IV (Fig. 6). We also observed concentrations slightly greater than background concentrations in unit VI and VIII (Fig. 6). Except for calcrete duricrust, the sediments of the Kalahari that are mostly sands that are carbonate poor (Wanke and Wanke, 2007), suggesting that if carbonates are derived from the local Kalahari watersheds, the source must be from calcrete. Alternatively, the carbonates could be supplied from the Okavango watershed and transported to the distal portions of the delta by the Okavango

River. Measurements of water chemistry of the Okavango River at the inlet into the Okavango Delta show water with relatively low pH between 5.5 and 6.5 (Akoko et al., 2012). River water with such low pH will dissolve particulate carbonate in transit and therefore it is unlikely that the Okavango River is a source of carbonate in the modern time. Although there is the possibility that in the past the Okavango River could bring carbonates from the upper watersheds, this is unlikely since the rocks in the upper watershed are composed primarily of ultra-mafic and felsic igneous rocks (Haddon and McCarthy, 2005). Assuming that the calcrete are derived from the local watersheds, the erosion of calcrete from the Okavango watershed will occur during a period of locally or regionally wet climate, as the highest concentration of carbonate of 2.5% is more than 10 times the background concentration of 0.2% in the sedimentary units at the study site. If a locally or regionally wet climate is required to supply high concentrations of carbonates, then it is possible to accumulate significant water within the study area to form a mega-lake. We interpret the high carbonate concentrations recorded in the sedimentary record of Unit IV as a mega-paleolake that formed within the distal portion of the Okavango Delta.

We observed a pronounced enrichment in the $\delta^{13}C_{TIC}$ in Unit IV which suggests the $\delta^{13}C$ is markedly different from that of the other portions of the sediment record (Units VIII, VII, VI, II and I) with predominantly low background TIC concentrations (Fig. 6). Calcrete duricrusts in the Kalahari analyzed for $\delta^{13}C_{TIC}$ and $\delta^{18}O_{TIC}$ by Ringrose et al. (2009) and Kampunzu et al. (2007) are shown in Figure 10. The $\delta^{13}C_{TIC}$ from the Ringrose et al. (2009) and Kampunzu et al. (2007) study ranged from -15.0 to +1.6‰ (VPDB) and the $\delta^{18}O$ ranged from 16.0 to 28.0‰ (VSMOW). The $\delta^{13}C$ of the carbonate

from the sedimentary section of the study site ranged from -9.0 to -3.6‰ (VPDB) and the $\delta^{18}O$ ranged from 19.0 to 35.0‰ (VSMOW). While the $\delta^{18}O_{TIC}$ from this study overlaps with those of the Ringrose et al. (2009) and Kampunzu et al. (2007) study, the $\delta^{13}C$ are clearly different from that of the averaged calcrete (Ringrose (2009): $\delta^{13}C = -2.2 \pm 4.4$‰; Kampunzu et al. (2007): $\delta^{13}C = -2.2$‰) except for Units IV and V. This suggests that the carbonates from Units I, II, III, VI, VII, and VIII in the sedimentary section are not directly derived from the calcrete from the local Kalahari watersheds. While the $\delta^{13}C$ of carbonates lie between isotopic values for freshwater carbonates ($\delta^{13}C$ as low as -15.0; Ringrose et al., 2009) and Kalahari calcrete ($\delta^{13}C$ as high as +1.6‰; Ringrose (2009)), it is possible that the $\delta^{13}C_{TIC}$ of the study site reflect a mixture of progressively increasing amounts of calcrete relative to the local freshwater carbonates. The TIC concentration data for Unit IV shows increasing TIC with an increasing shift toward isotopic values dominated by heavy carbon. In this case, the more positive $\delta^{18}O$ measured in the carbonates at the study site compared to local calcrete reflects perhaps re-equilibration with lake water.

The $\delta^{13}C$ of carbonates precipitated on an Okavango Delta island (19°32’49.13” S, 23°10’38.49”E) range from -5.1‰ to -3.0‰ (VPDB) and the $\delta^{18}O$ range from 29.5‰ to 32.0‰ (SMOW) (E. Atekwana, personal communication). The $\delta^{13}C$ is in the upper as that of carbonates from the study site, but the $\delta^{18}O$ is more positive compared to the carbonates from the study site (Fig. 10). This suggests that carbonates precipitating in the present day aquatic system of the Okavango have more positive $\delta^{18}O$ isotopic values. An alternative way of explaining the $\delta^{13}C$ and $\delta^{18}O$ of carbonates in Unit IV from the study area is from mixing carbonates from the local watershed with carbonates precipitated in

an aqueous environment such a lake. An analog for carbonates that precipitate in an aqueous environment in the Okavango is the islands where carbonates are precipitated. Since the same source of water that feeds the islands also likely feed the lakes, it can be assumed that carbonates precipitated from a lake will have similar $\delta^{13}C$ and $\delta^{18}O$ values to carbonates precipitated in modern day Okavango Delta islands (Fig. 10). The progressively increasing concentrations of TIC and increasing $\delta^{13}C$ of the carbonates at the bottom of Unit IV will fit such a mixing model. At the peak elevation of the lake, the $\delta^{13}C$ of the carbonates will be dominated by carbonates precipitated in the lake. We observe that at the highest TIC concentration in Unit IV, the $\delta^{13}C$ stabilizes to a value of about -3.5‰ which is in the range of that for carbonates precipitated on the Okavango Delta islands (Fig. 10). As lake levels decline, periodic supply of fresh water carbonate from the local watershed mixed with decreasing carbonate from lake precipitation will cause the $\delta^{13}C$ of the sedimentary carbonate to revert back to background $\delta^{13}C$ value of -7.0‰. Although this scenario appears possible, it is difficult to explain why only fresh water carbonates will be eroded from the local watershed as opposed to both fresh water carbonates and calcrete.

We also observe that although the concentrations of TIC in Unit V is rather low, the $\delta^{13}C$ also shows a pronounce increase relative to the $\delta^{13}C$ background values (Fig. 6). Unit V may also represent wet conditions, although lack of significant accumulation of TIC may indicate mostly low lake levels, and thus this unit may be a precursor to the mega-lake that subsequently developed in the region.

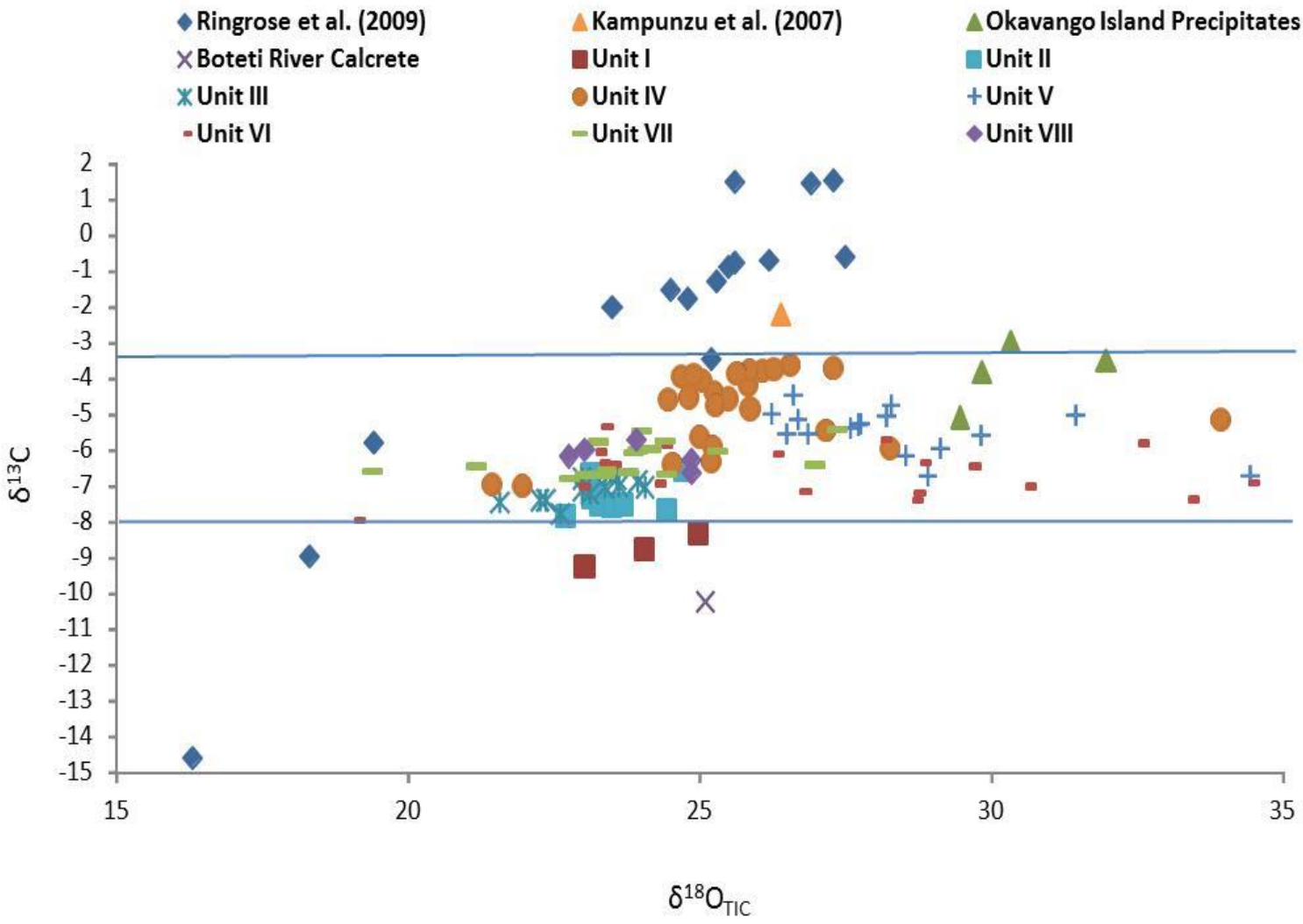

Fig. 10: Bivariate plot of $\delta^{13}C_{TIC}$ and $\delta^{18}O_{TIC}$ isotopes of all stratigraphic units at the study site compared to calcrete and island precipitates in the Okavango Delta.

5.4 TIC Comparisons

The TIC concentrations at the study site were compared to TIC concentrations in Lake Mababe (18º S to 19º S, 24º E to 24º30' E) (Gamrod, 2009), Lake Ngami (20º35'42.20"S, 22º34'17.06"E) (E. Atekwana, personal communication) and the Shorobe quarry (19°42.257'S, 23°43.119'E) (Fields, 2012) and shown in Figure 11. The Lake Ngami showed that paleolake Makgadikgadi began initiation between 42 and 40 thousand years ago (ka) inferred from inorganic and organic carbon content, various rare earth elements, and diatoms (Huntsman-Mapila et al., 2006). The initiation of the mega-paleolake is shown in blue at a depth of 4.5 meters in the Lake Ngami basin (Fig. 11) It is then noticed that after the initiation of the lake, there are two episodes of high concentrations of TIC shown in Lake Ngami and Lake Mababe sections. The Shorobe quarry and the study site are both located outside the lake basins in the lower Okavango Delta, and they show one episode of anomalously high TIC concentrations. This suggests that a mega-lake was present where the high TIC concentrations occur in the stratigraphic sections. These do not occur at the same depth because elevations of the mega-lake may vary at different location; however if each of these were constrained with time, we expect to see initiation of the lake occurring around the same time (42-40 ka).

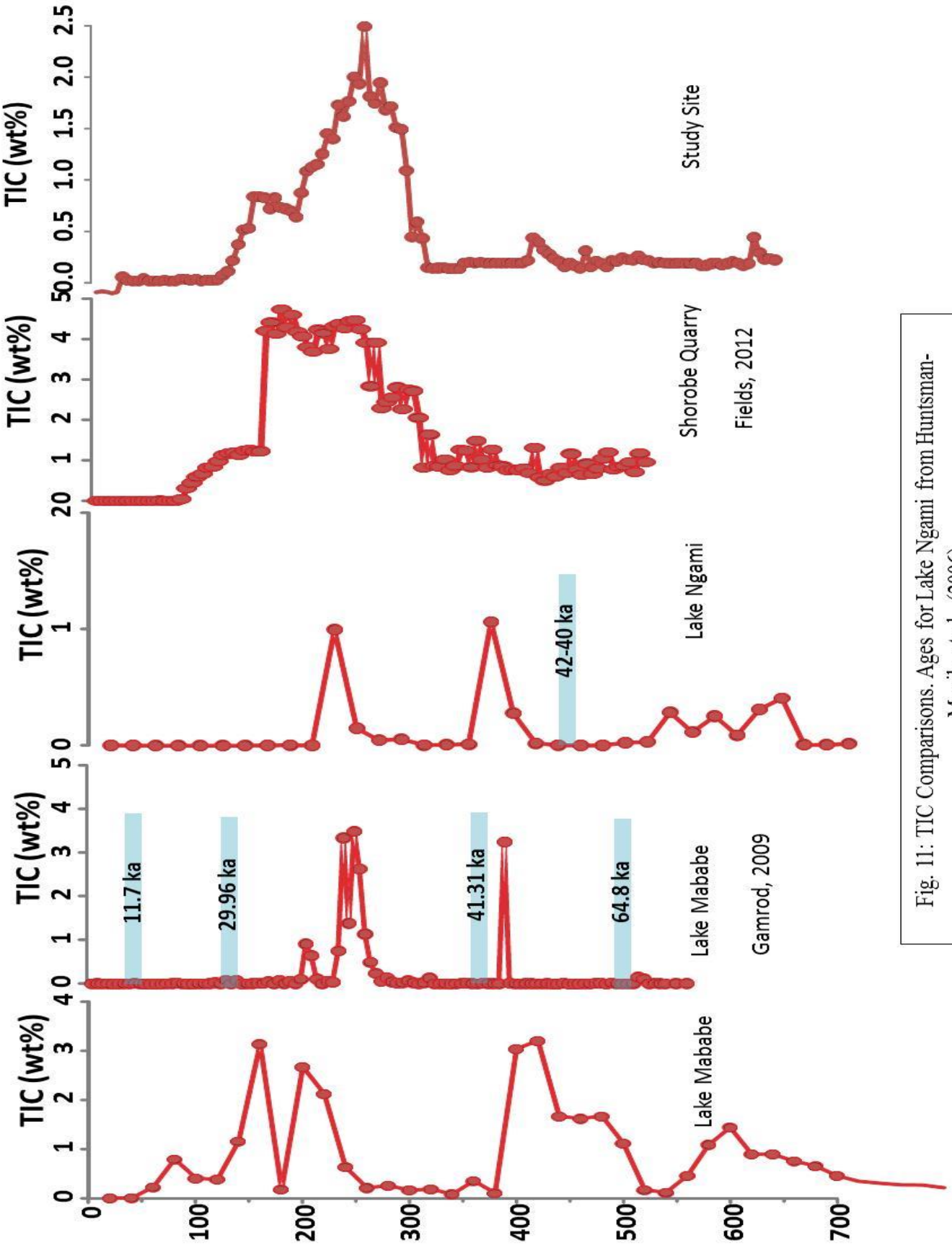

Fig. 11: TIC Comparisons. Ages for Lake Ngami from Huntsman-Mapila et al., (2006).

5.5 Variations in TOC Concentrations

Organic carbon can be used as an indicator of the presence or absence of vegetation within the watershed or in the aquatic environment (Boyle, 2001). TOC concentration represents the fraction of organic matter that escaped remineralization during sedimentation (Meyers and Teranes, 2001). Changes in vegetation in the watershed that supplies organic matter to a sedimentary basin, and organic matter production in the aquatic environment will be recorded in the TOC concentration. (Meyers and Teranes, 2001). Vegetation types in a watershed record change in climate and environmental conditions (Meyers and Lallier-Vergès, 1999). Alternating C_3 and C_4 plant types are used to depict wet and dry climate changes, respectively (Meyers and Lallier-Vergès, 1999).

Changes in the TOC can be due to the amount of organic matter transported into a basin, or from *in situ* production in a lake (Meyers and Lallier-Verges, 1999). There is an increase in TOC in units I, II, III, IV and VI (Fig. 6). The increase in TOC in each of these units could be from aquatic plants produced in a lake. Organic matter could also be transported to the study site and derived from the vegetation along the delta.

5.6 Variations in Biogenic Silica Concentrations

Biogenic silica was measured as a proxy for diatoms. The presence or absence of diatoms can be used as an indicator of lake levels (Kilham et al., 1986). Planktonic diatoms from Africa are used to interpret climatic conditions over the last 20,000 years (Kilham et al., 1986). The types of diatoms that exist depend on Si:P ratios and eutrophic conditions (Kilham et al., 1986). Since Silicon (Si) and Phosphorous (P) are dependent

on biological uptake, high Si:P ratios is often favored by diatoms. The availability of light and phosphorous depends on turbidity of the water and relative depths of mixing. Therefore, diatoms usually exist in eutrophic conditions with intense mixing within a lake (Kilham et al., 1986).

Diatoms were examined under a microscope at 400X to analyze relative abundance of diatoms, and were identified using Gasse (1986). Ten samples were analyzed allowing each unit to be represented. Microscopic examination of diatoms shows a high relative abundance of diatoms in units: I, IV, VI, and VIII compared to the other units (Fig. 12). Although the microscopic examination reflected the presence of diatoms, the study site did not produce high amounts of biogenic silica compared to other sites such as Lake Mababe. Biogenic silica concentrations at the study site range only from 1 E -04 to 6 E -04 weight % while biogenic silica at Lake Mababe ranged from 10 to 60 weight % (Teter, 2009).

Lake Mababe data indicated that diatom growth is dependent on availability of nutrients and lake water levels (Teter, 2009). The low abundance of biogenic silica at the study site (Fig. 6) may indicate that the lake was not stable for a long period of time, the diatoms were not well preserved, or nutrient levels were too low to produce diatoms. The presence of diatoms should be indicative of a lacustrine environment, but without identification of types of diatoms this cannot be conclusive.

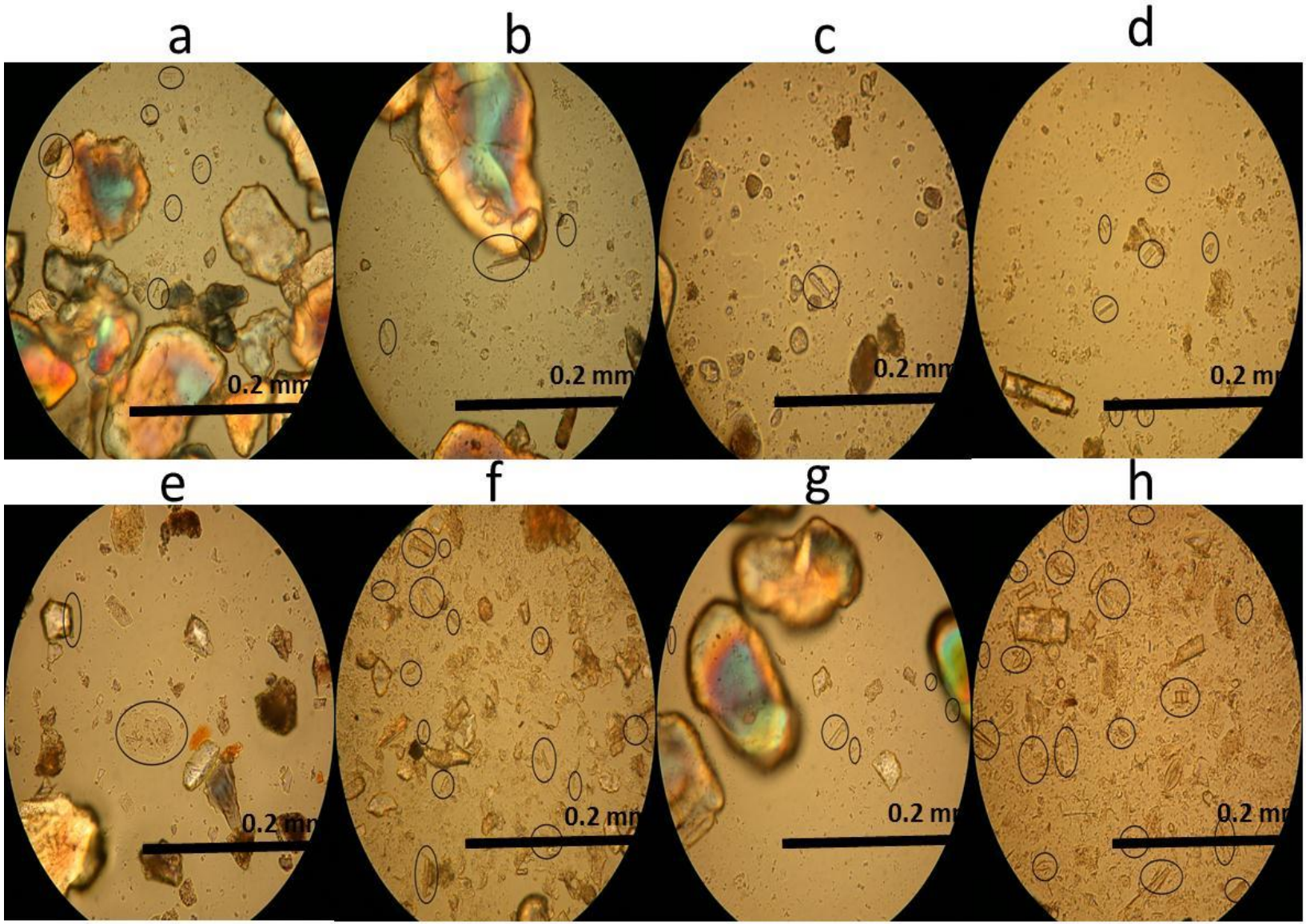

Fig. 12. Photographs of diatoms (circled in black). a) Unit I; 0-5 cm b) Unit II; 80-85 cm c) Unit III; 170-175 cm d) Unit IV; 275-280 cm e) Unit V; 330-335 cm f) Unit VI; 465-470 cm g) Unit VII; 565-570 cm h) Unit VIII; 635-640 cm

5.7 Sedimentation in the Lower Okavango Delta and its Bearing on Mega-paleolake Formation and Evolution

We interpreted the evolution of the stratigraphic section using sedimentary, geochemical and isotopic characteristics as one occurrence of a mega-paleolake. Beginning at the base of the section, unit VIII is indicative of a riverine flooded surface because of high clay and silt percentage, higher TOC and TIC concentrations, and higher relative abundance of diatoms. The environment changes in unit VII. Unit VII represents erosion of the local sand dunes due to predominance of sand size grains and moderately well sorted white sand. Units VI to IV illustrate an increase in clay and silt percentages which we attribute to the initiation of the mega-lake. The high concentration of TIC in unit IV represents the mega-lake episode derived from either erosion of the local calcretes during a wet period, or production of carbonates in the lake. Unit III to unit I is interpreted to represent the decline of the mega-lake.

CHAPTER 6

CONCLUSIONS

The results of this study provide evidence of one mega-paleolake episode that occurred and is recorded in Unit IV of the stratigraphic section at the study site. The variations in grain size distribution and sorting were used to interpret depositional environments that are recorded in the stratigraphic section. Predominance of clay and silt is typical of lacustrine environments. Clay and silt that is supplied to the area is sourced from the catchment in Angola. The sediments from Angola could only be transported to the distal portion of the delta during a wet climate. Therefore, an increase of the clay and silt fractions at the site is representative of a wet period that could create a mega-lake. It was concluded that lacustrine sedimentation was recorded at the study site indicating possible presence of a mega-lake.

To further define the occurrence of a mega-paleolake within the stratigraphic section, geochemical and isotopic proxies were used. In Unit IV the $\delta^{13}C_{TIC}$ are enriched and reach -3.5‰ relative to the other background values of -7‰. Since it is becoming closer to the $\delta^{13}C_{TIC}$ of local Kalahari calcretes which average -2.2‰, it is likely that during this time a high influx of water eroded the calcretes from the local watershed into the mega-lake. Comparisons of TIC concentrations with data from sediments from

Lake Ngami and Lake Mababe show anomalously higher concentrations of TIC after the initiation of paleolake Makgadikgadi. This high concentration can then be related to the occurrence of a mega-lake. Therefore the high concentration of TIC (up to 2.5%) in Unit IV relative to other units represents either erosion of the surrounding calcretes that was subsequently washed into the mega-lake that existed, or carbonates produced in the mega-lake. This suggests that a mega-lake occurred in Unit IV of the stratigraphic section.

Unit V shows an enrichment in $\delta^{13}C_{TIC}$ which could represent wet conditions because the $\delta^{13}C_{TIC}$ is beginning to reach values close to those of the local Kalahari calcretes. The lack of significant amounts of TIC preserved in Unit V may indicate low lake levels and thus this unit may be a precursor to the mega-lake that subsequently developed in the region recorded in Unit IV.

Identifying mega-paleolake formation beyond the Makgadikgadi, Ngami and Mababe lake basins is important in predicting future climate changes in Northern Botswana. Events leading up to the formation of a lake can cause flooding and devastation to the people that live near the Okavango Delta. Unraveling the evolution of mega-paleolakes helps to predict devastating climatic changes.

CHAPTER 7

FUTURE WORK

The spatial extent and timing of a mega-paleolake at the distal portion of the Okavango Delta can be further refined. Age constraints of the sediments are important in order to establish the timing and evolution of the mega-paleolakes from sedimentary records. Age constraints from Optically Stimulated Luminescence (OSL) dating can provide timing of the deposition of sediment which can be used to determine the timing of a mega-lake. The timing can be compared with other Makgadikgadi lake highstands suggested by previous studies (Shaw, 1988; Shaw et al., 2003; Burrough and Thomas, 2008; Burrough et al., 2009a; 2009b). The event associated with an increase in carbonate material found in this study and other studies in Lake Ngami, Mababe Lake and areas surrounding the Okavango Delta alluvial fan, needs to be constrained with time. If it is the same event, it may have implications for the timing of paleolake formation.

It is clear from the $\delta^{13}C$ of TIC that the carbonate material is not coming from a single source. The source of inorganic carbon can be further investigated. Incorporating stable nitrogen (N) isotopes into the dataset can help constrain sources of organic matter. C/N ratios are used to differentiate between aquatic and land sources (Meyers and Teranes, 2001). More geomorphological and geochemical studies in the area can help

define the extent and nature of the lake that formed in this area.

Additional investigation into the types of diatom communities throughout the section can help determine nutrient conditions and high and low lake levels. Scanning electron microscope (SEM) imaging can be done to identify the types of diatoms, and can be used to help further define the lake episode(s).

REFERENCES

Ahlbrandt, T. S. and Fryberger, S. G. 1982: Introduction to Eolian Deposits. Edited by Peter A. Scholle and Darwin Spearing. *AAPG Memoir* 33. 11-48.

Akoko, E, Atekwana, E.A., Cruse, A.M., Molwalefhe, L, and Masamba, W.R.L. 2012: River-wetland interaction and carbon cycling in a semi-arid riverine system: the Okavango Delta, Botswana. *Biogeochemistry*.

Boyle, J.F. 2001: Inorganic Geochemical Methods in Palaeoliminology. Edited by W.M. Last and J.P. Smol. Tracking Environmental Change Using Lake Sediments Vol. 2: Physical and Geochemical Methods, 83-141.

Bufford, K. M, Atekwana, E.A., Abdelsalam, M.G., Shemang, E, Atekwana, E.A., Mickus, K, Moidaki, M, Modisi, M.P. and Molwalefhe, L. 2012: Geometry and faults tectonic activity of the Okavango Rift Zone, Botswana: Evidence from magnetotelluric and electrical resistivity tomography imaging. *Journal of African Earth Sciences,* 65, 61-71.

Burrough, S.L. and Thomas, D.S.G. 2008: Late Quaternary lake-level fluctuations in the Mababe Depression: Middle Kalahari paleolakes and the role of Zambezi inflows. *Quaternary Research*, 388-403.

Burrough, S.L, Thomas, D.S.G., and Bailey, R.M. 2009a: Mega-Lake in the Kalahari: A Late Pleistocene record of the Palaeolake Makgadikgadi system. *Quaternary Science Reviews*, 1392-1411.

Burrough, S.L., Thomas, D.S.G., and Singarayer, Joy S. 2009b: Late Quaternary hydrological dynamics in the Middle Kalahari: Forcing and feedbacks. *Earth Science Reviews*, 313-326.

Davis, R.A. 1983: Depositional Systems. 141-168.

Dean, W.E. and Fouch, T.D. 1983: Lacustrine Environment. Edited by Peter A. Scholle, Don G. Bebout, and Clyde H. Moore. *AAPG Memoir 33*, 98-130.

Emrich, K., Ehhalt, D.H. and Vogel, J.C. 1970: Carbon Isotope Fractionation during the precipitation of calcium carbonate. *Earth and Planetary Science Letters*, 363-371.

Fields, A. 2012: Investigating Paleoflooding in the Okavango Delta, Northwest Botswana from Sedimentary Records, M.S. Thesis. Oklahoma State University.

Folk, R.L. and Ward. W.C., 1957. Brazos River Bar: A study in the significance of grain size parameters. *Journal of Sedimentary Petrology*. 27, 3-26.

Folk, R.L. 1974: Petrology of sedimentary rocks. 182 p.

Friedman, G.M. 1967: Dynamic processes and statistical parameters compared for size frequency distribution of beach and river sands. *Journal of Sedimentary Petrology* Vol. 37, 327-354.

Gamrod, J. 2009: Paleoliminological records of environmental change preserved in paleo-lake Mababe, Northwest Botswana, M.S. Thesis. Oklahoma State University.

Gasse, F. 1986: East African diatoms taxonomy, ecological distribution.

Goudie, A.S. 2005: The drainage of Africa since the Cretaceous. *Geomorphology*, 437-456.

Haddon, I.G. and McCarthy, T.S. 2005: The Mesozoic-Cenozoic interior sag basins of Central Africa: The Late-Cretaceous-Cenozoic Kalahari and Okavango basins. *Journal of African Sciences*, 316-333.

Hamandawana, H., Chanda, R. and Eckardt, F. 2008: Reappraisal of contemporary perspectives on climate change in southern Africa's Okavango Delta sub-region. *Journal of Arid Environments*, 1709-1720.

Hassan, K.M. and Spalding, R.F. 2001: Hydrogen isotope values in lacustrine kerogen. *Chemical Geology*. 175, 713-721.

Holmgren, K. and Shaw, P. 1997: Palaeoenvironmental reconstruction from near-surface pan sediments: an example from Lebatse Pan, Southeast Kalahari, Botswana. *Geografiska Annaler* 79, 83-93.

Huntsman-Mapila, P., Kampunzu, A.B., Vink, B. and Ringrose, S. 2005: Cryptic indicators of provenance from the geochemistry of the Okavango Delta sediments, Botswana. *Sedimentary Geology*, 174 123-148.

Huntsman-Mapila, P., Ringrose, S., Mackay, A.W., Downey, W.S., Modisi, M., Coetzee, S.H., Tiercelin, J.-J., Kampunzu, A.B. and Vanderpost, C. 2006: Use of geochemical and biological sedimentary record in establishing palaeo-environments and climate change in the Lake Ngami basin, NW Botswana. *Quaternary International*, 148, 51-64.

Kampunzu, A.B., Ringrose, S., Huntsman-Mapila, P., Harris, C., Vink, B.W. and Matheson, W. 2007: Origins and palaeo-environments of Kalahari duricrusts in the Moshaweng dry valleys (Botswana) as detected by major and trace element composition. *Journal of African Earth Sciences*, 28, 199-221.

Kilham, P., Kilahm, S.S., and Hecky, R.E. 1986: Hypothesized resource relationships among African planktonic diatoms. *Limonology Oceanography,* 31, 1169-1181.

Kinabo, B.D., Atekwana, E.A., Hogan, J.P., Modisi, M.P., Wheaton, D.D., and Kampunzu, A.B. 2007: Early structural development of the Okavango rift zone, NW Botswana. *Journal of African Earth Sciences* 48, 125-136.

Krishnamurthy, R. V., Atekwana, E.A., and H. Guha. 1997: A simple, inexpensive carbonate –phosphoric acid reaction method for the analysis of carbon and oxygen isotopes of carbonates: *Analytical Chemistry*, 4256-4258.

McCarthy, T.S., Rogers, K.H., Stanistreet, I.G., Ellery, W.N., Cairncross, B., Ellery, K. and Grobicki, T.S.A., 1988: Features of channel margins in the Okavango Delta. *Palaeoecology Africa*, 19: 3-14.

McCarthy, T.S., Stanistreet, I.G. and Cairncross, B. 1991: The sedimentary dynamics of active fluvial channels on the Okavango fan, Botswana. *Sedimentology*, 38, 471-487.

McCarthy, T.S., Ellery, W.N. and Stanistreet, I.G. 1992: Avulsion mechanisms on the Okavango fan, Botswana: the control of a fluvial system by vegetation. *Sedimentology* 39, 779-795.

McCarthy, T.S., and Ellery, W.N. 1995: Sedimentation on the distal reaches of the Okavango Fan, Botswana, and its bearing on calcrete and silcrete (Ganister) formation. *Journal of Sedimentary Research*, Vol. A65 No. 1, 77-90.

McCarthy, B.M., Bloem, A., Ellery, W.N., Heister, H., Merry, C.L., Ruther, H. and Sternberg, H. 1997: The gradient of the Okavango fan, Botswana, and its sedimentological and tectonic implications. *Journal of African Earth Sciences* Vol. 24, 65-78.

McCarthy, T.S. and Ellery, W.N. 1998: The Okavango Delta. 157-182.

Meyers, P.A. and Lallier-Vergès, E. 1999: Lacustrine sedimentary organic matter records of Late Quaternary paleoclimates. *Journal of Paleoliminology*, 21, 345-372.

Meyers, P.A. and Teranes, J.L. 2001: Sediment Organic Matter. Tracking Environmental Change Using Lake Sediments. Vol. 2, 239-269.

Milzow, C., Kgotlhang, L., Bauer-Gottwein, P., Meier, P. and Kinzelbach, W. 2009: Regional review: the hydrology of the Okavango Delta, Botswana-processes, data and modeling. *Hydrogeology Journal* 17, 1297-1328.

Modisi, M.P., Atekwana, E.A., Kampunzu, A.B., and Ngwisanyi, T.H. 2000: Rift kinematics during the incipient stages of continental extension: Evidence from the nascent Okavango rift basin, northwest Botswana. *Geology* 28, 939-942.

Mortlock, R.A. and Froelich, P.N., 1989: A simple method for the rapid determination of biogenic opal in pelagic marine sediments. *Deep-Sea Research* 36, 1415-1426.

Nash, D.J. and McLaren, S.J. 2003: Kalahari valley calcretes: their nature, origins, and environmental significance. *Quaternary International* 111, 3-22.

Nichols, G.J. and Fisher, J.A. 2007: Processes, facies and architecture of fluvial distributary system deposits. *Sedimentary Geology*, 195, 75-90.

Nilsen, T.H. 1982: Alluvial Fan Deposits. Edited by Peter A. Scholle and Darwin Spearing. *AAPG Memoir* 31. 49-86.

Otvos, E.G. 2000: Beach ridges- definitions and significance. *Geomorphology* 32, 83-108.

Ringrose, S., Downey, B., Genecke, D., Sefe, F. and Vink, B. 1999: Nature of sedimentary deposits in the western Makgadikgadi basin, Botswana. *Journal of Arid Environments*, 375-397.

Ringrose, S., Harris, C., Huntsman-Mapila, P., Vink, B.W., Diskins, S., Vanderpost, C. and Matheson, W. 2009: Origins of strandline duricrusts around the Makgadikgadi Pans (Botswana Kalahari) as deduced from their chemical and isotope composition. *Sedimentary Geology* 219, 262-279.

Shaw, P. 1988: After the Flood: The Fluvio-Lacustrine Landforms of Northern Botswana. *Earth Science Reviews,* 449-456.

Shaw, P.A., Bateman, Mark D., Thomas, David S.G., Davies, Frances 2003: Holocene fluctuations in Lake Ngami, Middle Kalahari: chronology and responses to climatic change. *Quaternary International*, 23-35.

Stanistreet, I.G. and McCarthy, T.S. 1993: The Okavango fan and the classification of subaerial fan systems. *Sedimentary geology*, 85, 115-133.

Teter, K., 2009: Paleoenvironmental reconstruction of Paleolake Mababe, northwestern Botswana from sediment chemistry and biological productivity data, M.S. Thesis. Oklahoma State University.

Thomas, D.S.G. 1987: Discrimination of depositional environments using sedimentary characteristics in the Mega Kalahari, central southern Africa. *Desert Sediments: Ancient and Modern,* 293-306.

Thomas, D.S.G. and Shaw, P.A. 1988: Late Cainozoic Drainage Evolution in the Zambezi Basin: Geomorphological Evidence from the Kalahari Rim. *Journal of African Earth Sciences,* 611-618.

Thomas, D.S.G and Shaw, P.A. 1992: The Zambezi River: tectonism, climatic change and drainage evolution- is there really evidence for a catastrophic flood? A discussion. *Palaeogeography, Palaeoclimatology, Palaeoecology*, 175-182.

UCL Department of Geography. Diatom Preparation. <http://www.geog.ucl.ac.uk/about-the-department/support-services/laboratory/laboratory-methods/lake-sediment-analysis/diatom-preparation(1/24/2013).

Verardo, D.J., Froelich, P.N., and McIntyre, A. 1989: Determination of organic carbon and nitrogen in marine sediments using the Carlo Erba NA-1500 Analyzer. *Deep Sea Research*. Vol. 37, No. 1, 157-165.

Wanke, H. and Wanke, A. 2007: Lithostratigraphy of the Kalahari Group in northeastern Namibia. *Journal of African Earth Sciences*, 48, 314-328.

White, D.C. 1966: Coulometric titration of carbon dioxide on the micro scale. *Talanta*, 13, 1303-1311.

APPENDIX

A1

Sample depth (cm)	Munsell number	Munsell Color	% Clay	% Silt	% Sand
5	3/210YR	very dark grayish brown	4.728	13.43131	81.84
10	3/210YR	very dark grayish brown	7.094	22.25265	70.65
15	3/210YR	very dark grayish brown	9.63	34.96592	55.415
20	3/210YR	very dark grayish brown	4.455	15.71949	79.825
25	4/210YR	dark grayish brown	5.2085	19.98153	74.81
30	4/210YR	dark grayish brown	3.947	15.06661	81.085
35	4/210YR	dark grayish brown	4.338	17.52572	78.14
40	4/210YR	dark grayish brown	3.331	13.52398	83.145
45	4/210YR	dark grayish brown	3.329	14.21571	82.455
50	4/210YR	dark grayish brown	2.715	10.8083	86.48
55	4/210YR	dark grayish brown	2.403	9.998714	87.595
60	4/210YR	dark grayish brown	2.9	11.8843	85.215
65	4/210YR	dark grayish brown	5.7615	22.02134	72.215
70	4/210YR	dark grayish brown	9.595	42.17478	48.23
75	4/210YR	dark grayish brown	15.24	48.93231	35.83
80	4/210YR	dark grayish brown	13.445	37.0301	48.025
85	4/210YR	dark grayish brown	14.58	43.99177	41.425
90	4/210YR	dark grayish brown	9.6655	30.53583	59.8
95	4/210YR	dark grayish brown	19.335	57.21482	23.45
100	4/210YR	dark grayish brown	13.49	44.66955	41.84
105	4/210YR	dark grayish brown	8.1215	26.48447	65.395
110	4/210YR	dark grayish brown	8.4585	29.46241	62.08
115	4/210YR	dark grayish brown	9.376	34.62055	56.005
120	4/210YR	dark grayish brown	8.9335	31.24425	59.82
125	4/210YR	dark grayish brown	5.466	17.29706	77.235
130	5/210YR	grayish brown	7.44	20.56544	73.49
135	5/210YR	grayish brown	4.4405	16.14169	79.42
140	5/210YR	grayish brown	7.5755	24.6862	67.735
145	6/210YR	light brownish gray	4.774	16.42101	81.805
150	6/210YR	light brownish gray	6.1345	22.3769	71.49
155	6/210YR	light brownish gray	7.5245	31.01581	61.46
160	6/210YR	light brownish gray	4.734	21.02949	74.235
165	6/210YR	light brownish gray	5.917	29.09876	64.98
170	6/210YR	light brownish gray	5.025	28.39231	66.58
175	6/210YR	light brownish gray	4.9445	33.37948	61.68

180	6/210YR	light brownish gray	7.262	59.54457	33.19
185	6/210YR	light brownish gray	5.864	40.98497	53.15
190	6/210YR	light brownish gray	3.164	24.83606	72
195	6/310YR	pale brown	2.435	17.58018	79.985
200	6/310YR	pale brown	2.573	23.96788	73.455
205	7/310YR	very pale brown	2.659	24.55527	72.785
210	8/210YR	very pale brown	3.0835	27.89682	69.02
215	8/210YR	very pale brown	3.359	19.55281	77.09
220	8/210YR	very pale brown	4.09	27.01184	68.9
225	8/210YR	very pale brown	3.9695	22.58636	73.445
230	8/210YR	very pale brown	2.3215	13.53256	84.15
235	8/210YR	very pale brown	3.063	21.50352	75.435
240	8/210YR	very pale brown	2.846	17.41363	79.605
245	8/210YR	very pale brown	3.163	14.19042	82.645
250	8/210YR	very pale brown	3.842	23.77429	72.385
255	8/210YR	very pale brown	5.7955	33.92487	60.28
260	8/210YR	very pale brown	4.125	23.68967	72.185
265	8/210YR	very pale brown	3.4395	18.02177	78.535
270	7/4 10YR	very pale brown	4.162	22.06439	73.775
275	7/4 10YR	very pale brown	5.0285	27.0872	67.885
280	7/4 10YR	very pale brown	2.6725	16.23006	81.1
285	7/4 10YR	very pale brown	4.9105	31.08373	64.005
290	7/4 10YR	very pale brown	4.19	25.58795	70.485
295	7/4 10YR	very pale brown	6.7125	40.93043	55.685
300	7/4 10YR	very pale brown	4.1255	29.50376	66.37
305	7/4 10YR	very pale brown	3.9375	29.60615	66.455
310	7/4 10YR	very pale brown	4.596	33.63029	61.77
315	7/4 10YR	very pale brown	3.694	26.13996	70.17
320	7/4 10YR	very pale brown	3.747	29.02212	67.23
325	7/4 10YR	very pale brown	3.491	24.58931	71.92
330	7/4 10YR	very pale brown	3.4975	23.3914	73.115
335	7/4 10YR	very pale brown	3.7375	26.55185	69.71
340	7/4 10YR	very pale brown	4.2405	28.60762	67.155
345	7/4 10YR	very pale brown	3.551	22.46686	73.98
350	7/4 10YR	very pale brown	5.492	35.79983	58.71
355	7/4 10YR	very pale brown	6.1605	37.95666	55.885
360	7/4 10YR	very pale brown	4.406	25.2751	70.32
365	7/4 10YR	very pale brown	3.6955	27.74116	68.56
370	7/3 10YR	very pale brown	2.8815	18.23154	78.89
375	7/3 10YR	very pale brown	5.133	33.77679	61.09
380	7/3 10YR	very pale brown	4.4295	29.48814	66.08
385	7/3 10YR	very pale brown	4.563	31.84692	63.59

390	8/2 10YR	very pale brown	3.0955	16.86986	80.035
395	8/2 10YR	very pale brown	2.8425	16.10994	81.05
400	8/2 10YR	very pale brown	2.757	17.45303	79.79
405	8/2 10YR	very pale brown	4.442	34.36898	61.19
410	8/2 10YR	very pale brown	3.5905	22.91703	73.495
415	7/3 10YR	very pale brown	4.2855	27.68795	68.025
420	7/3 10YR	very pale brown	7.696	54.15762	38.15
425	7/3 10YR	very pale brown	5.632	37.79165	56.575
430	6/2 10YR	light brownish gray	5.8545	42.10118	52.045
435	6/2 10YR	light brownish gray	4.8345	40.77911	54.385
440	8/2 10YR	very pale brown	2.8525	18.62449	78.525
445	8/2 10YR	very pale brown	1.9775	10.16086	87.86
450	8/2 10YR	very pale brown	1.9205	9.003192	89.075
455	8/2 10YR	very pale brown	2.5475	12.12266	85.33
460	8/2 10YR	very pale brown	3.131	24.20048	72.67
465	8/2 10YR	very pale brown	3.604	25.43837	70.955
470	10YR 7/3	very pale brown	5.8225	44.17262	50.005
475	10YR 7/3	very pale brown	5.451	41.20801	54.845
480	10YR 7/3	very pale brown	5.722	38.26282	56.015
485	10YR 7/3	very pale brown	6.202	52.07456	41.725
490	10YR 8/2	very pale brown	2.584	14.09662	83.32
495	10YR 8/2	very pale brown	2.2105	12.05391	85.735
500	10YR 8/2	very pale brown	2.2895	10.74548	86.965
505	10YR 7/3	very pale brown	3.1495	26.90741	69.945
510	10YR 7/3	very pale brown	4.6085	37.8331	57.555
515	10YR 7/3	very pale brown	3.856	27.3529	68.79
520	10YR 7/3	very pale brown	5	39.00071	56
525	10YR 7/3	very pale brown	3.4475	22.73974	73.81
530	10YR 8/1	white	2.504	15.87481	81.625
535	10YR 8/1	white	1.6635	9.5877	88.75
540	10YR 8/1	white	1.578	6.908053	91.515
545	10YR 8/1	white	1.5845	6.376418	92.04
550	10YR 8/1	white	1.2985	4.277341	94.425
555	10YR 8/1	white	1.2375	4.044368	94.72
560	10YR 8/1	white	1.164	3.45597	95.38
565	10YR 8/1	white	1.1085	2.871869	96.02
570	10YR 8/1	white	1.159	3.272634	95.57
575	10YR 8/1	white	1.1085	2.753119	96.14
580	10YR 8/1	white	1.141	2.953862	95.905
585	10YR 8/1	white	1.1835	3.149114	95.67
590	10YR 8/1	white	1.272	3.632589	95.095
595	10YR 8/1	white	1.524	4.331749	94.14

600	10YR 8/1	white	1.409	3.905299	94.685
605	10YR 8/1	white	1.3335	3.540373	95.125
610	10YR 8/1	white	1.4095	4.169631	94.425
615	10YR 8/2	very pale brown	1.6585	5.039145	93.305
620	10YR 8/2	very pale brown	1.6455	4.681795	93.675
625	10YR 8/2	very pale brown	1.791	7.791743	89.915
630	10YR 4/2	dark grayish brown	13.545	60.39074	26.065
635	10YR 4/3	dark grayish brown	14.615	64.62482	20.76
640	10YR 5/2	grayish brown	8.733	48.82678	41.94
645	10YR 6/3	pale brown	7.0835	34.525	58.39
650	10YR 8/2	very pale brown	1.735	6.614989	91.65

APPENDIX

A2

Moment Mean	Moment Standard Deviation for grain size in Ø	Moment Skewness	Graphic Mean in Ø	Graphic Standard Deviation for Mean Grain in Ø	Graphic Skewness
3.198	1.5435	2.363	2.992	1.407	0.027
3.571	1.7825	1.671	3.805	1.958	-0.0258
4.233	2.0535	0.89935	4.306	2.13	0.1245
3.343	1.512	2.329	3.474	1.738	-0.0314
3.69	1.678	1.845	3.315	1.691	0.0673
3.171	1.5265	2.188	3.079	1.467	0.0391
3.419	1.5085	2.204	3.657	1.901	-0.0125
3.149	1.4743	2.274	2.859	1.355	0.0894
3.182	1.432	2.357	3.17	1.57	0.0288
3.035	1.3175	2.709	2.725	1.299	0.1281
3.016	1.2655	2.768	2.708	1.198	0.135
3.187	1.3635	2.568	2.854	1.3122	0.0905
3.853	1.814	1.5535	3.139	1.417	0.0794
4.368	1.8785	0.5675	4.096	2.056	0.1492
5.023	2.077	0.712	5.073	2.011	0.4729
3.901	1.994	0.8415	4.719	2.17	0.3728
4.675	2.151	0.7425	5.429	2.236	0.7451
3.876	1.9005	1.379	4.547	2.216	0.2819
6.135	1.949	0.428	6.126	2.129	0.799
4.179	1.972	1.011	4.78	2.199	0.3829
3.513	1.81	1.6355	3.995	2.057	0.1624
3.848	2.005	1.1535	4.135	2.146	0.0115
4.066	1.983	1.093	4.415	2.185	0.1502
3.713	1.962	1.1945	4.236	2.146	0.0861
3.457	1.573	2.173	3.813	1.978	-0.0519
3.65	1.6925	1.863	3.504	1.753	0.01922
3.178	1.448	2.4205	3.273	1.522	-0.0002
3.623	1.804	1.658	3.94	1.972	-0.0202
3.061	1.301	2.825	3.279	1.393	0.08276
3.924	1.562	2.201	3.582	1.583	0.0613
4.078	1.6975	1.7385	4.371	2.093	0.1828
3.523	1.6185	1.894	3.521	1.685	-0.0283
3.926	1.7785	1.4465	3.839	1.906	0.0552
3.571	1.6935	1.48	3.798	1.909	-0.0017
3.699	1.678	1.3975	3.929	1.888	0.1182
5.027	1.6565	1.0075	5.234	1.694	0.4499
4.259	1.773	1.089	4.242	1.909	0.3122
3.506	1.45	1.9225	3.588	1.604	0.0516

3.129	1.341	2.254	3.155	1.399	0.327
3.369	1.4035	1.8385	3.289	1.443	0.0451
3.439	1.4525	1.84415	3.493	1.533	0.0616
3.634	1.5355	1.5875	3.456	1.603	0.0895
3.581	1.505	1.981	3.655	1.699	0.0498
3.308	1.44	2.128	3.214	1.503	0.0046
3.256	1.551	1.997	3.643	1.793	0.0625
3.043	1.2735	2.5655	2.891	1.318	0.0395
3.339	1.497	1.8565	3.139	1.417	0.0161
3.144	1.3325	2.551	3.343	1.539	0.0278
3.158	1.5355	2.187	2.812	1.305	0.0489
3.577	1.5165	1.82	3.386	1.681	0.01848
3.926	1.752	1.4	4.106	2.026	0.1394
3.556	1.545	1.962	3.739	1.891	-0.0152
3.208	1.608	1.891	3.123	1.528	-0.0044
3.4	1.623	1.78	3.593	1.909	-0.0263
3.854	1.682	1.609	3.776	1.899	0.0349
3.247	1.5955	1.781	3.191	1.469	0.0329
4.279	1.582	1.6685	3.696	1.629	0.2338
3.417	1.7005	1.416	3.205	1.468	0.0121
4.345	1.8095	1.122	4.539	2.035	0.4859
3.621	1.617	1.502	3.796	1.837	0.0462
3.605	1.6435	1.46	3.674	1.806	0.0331
3.85	1.744	1.2995	3.869	1.846	0.1053
3.365	1.5745	1.661	3.592	1.786	0.0118
3.668	1.5615	1.6235	3.749	1.809	0.0695
3.291	1.5235	1.822	3.327	1.522	0.0448
3.38	1.538	1.834	3.613	1.788	-0.0318
3.538	1.6185	1.5765	3.52	1.716	-0.0059
3.784	1.611	1.676	3.811	1.869	0.0628
3.503	1.5795	1.7775	3.413	1.659	-0.0139
3.457	1.5045	2.002	3.486	1.716	-0.0111
3.513	1.7305	1.1335	4.026	1.945	0.2343
3.732	1.7175	1.4865	3.376	1.638	0.0336
3.58	1.5795	1.5685	3.7114	1.786	0.0228
3.1509	1.3385	2.3615	3.274	1.479	-0.0015
3.928	1.74	1.351	4.063	2.032	0.1528
3.971	1.7077	1.407	3.832	1.872	0.0544
3.4606	1.5735	1.6447	4.035	1.77	0.2659
3.1079	1.325	2.4705	3.152	1.384	-0.0258
3.2049	1.2345	2.6825	3.284	1.307	-0.0029
3.36	1.285	2.428	3.254	1.2702	0.0078

4.201	1.7885	0.983	3.619	1.444	0.1318
3.352	1.465	2.06925	3.731	1.698	0.0236
3.676	1.718	1.338	3.733	1.764	-0.0284
5.003	1.6565	0.409	4.539	1.9028	0.284
3.719	1.747	0.4565	4.151	1.9201	0.2407
3.656	1.7435	1.174	4.379	1.844	0.1799
4.142	1.7245	0.923	4.066	1.872	0.201
3.279	1.404	2.133	3.199	1.449	0.0415
3.105	1.1505	2.9425	3.376	1.375	0.1146
2.914	1.1455	3.1645	2.687	1.0359	0.1024
3.22	1.332	2.6245	2.859	1.186	0.0378
1.715	1.373	2.33	3.045	1.326	0.0785
3.588	1.479	1.8365	3.887	1.819	-0.0092
5.029	1.8085	0.4425	4.128	1.638	0.2979
3.507	1.5955	1.6115	4.123	1.828	0.2327
4.204	1.766	1.1733	4.423	1.976	0.2739
4.302	1.7225	0.691	4.813	1.87	0.4866
3.346	1.298	2.4175	4.103	1.375	0.1608
3.093	1.1725	2.873	2.932	1.212	0.0942
2.984	1.153	3.0685	2.876	1.978	0.0489
3.874	1.7285	1.1585	3.12	1.265	0.0864
3.799	1.742	0.2734	3.866	1.805	0.039
3.7001	1.6825	1.4735	3.826	1.832	-0.0022
4.0119	1.7565	0.9835	3.883	1.881	0.1082
3.192	1.583	1.6495	3.473	1.424	0.1352
3.185	1.0885	3.0185	3.335	1.253	0.0113
3.037	0.931	3.726	2.989	0.851	0.0452
2.988	0.918	4.037	2.917	0.742	0.0645
3.007	0.912	4.0735	2.868	0.7478	0.0774
2.896	0.8215	4.0735	2.783	0.64	0.1301
2.808	0.8355	4.543	2.704	0.642	0.1296
2.787	0.813	4.709	2.663	0.5617	0.1727
2.791	0.762	5.056	2.666	0.5338	0.1812
2.809	0.774	4.9705	2.658	0.576	0.1528
2.791	0.7535	5.132	2.667	0.536	0.1826
2.814	0.7555	5.0945	2.685	0.5359	0.1953
2.863	0.7725	4.96	2.751	0.5398	0.1863
2.903	0.803	4.8	2.774	0.5779	0.1492
2.906	0.905	4.363	2.756	0.6042	0.1443
2.903	0.8125	4.7495	2.781	0.6349	0.1225
2.9068	0.8149	4.758	2.784	0.558	0.1696
2.9447	0.8395	4.5495	2.829	0.6136	0.1149

2.999	0.9315	4.173	2.843	0.664	0.1095
2.981	0.896	4.3435	2.846	0.7062	0.1114
3.011	1.119	3.396	2.82	0.946	0.0904
5.001	2.009	0.3045	5.46	1.291	0.3733
5.449	1.9955	0.04	5.69	2.224	0.8669
4.921	2.0215	0.378	5.286	2.069	0.7735
3.855	1.823	1.283	4.231	2.079	0.1748
2.965	0.98895	3.7715	2.813	0.7676	0.0802

APPENDIX

A3

Magnetic Susceptibility	TIC wt %	TOC wt %	$\delta^{13}C_{TIC}$	$\delta^{18}O_{TIC}$	Dry buk density g/cm3	Biogenic Silica (uM)
0.00000006	-0.095	0.675	-9.233	23.029	1.64	0.058
0.00000006	-0.086	0.926			1.69	0.023
0.00000007	-0.091	0.714	-8.761	24.044	1.65	0.058
0.00000006	-0.105	0.453			1.67	0.064
0.00000007	-0.092	0.633			1.70	0.064
0.00000006	0.056	0.475			1.70	0.063
0.00000006	0.024	0.509	-8.318	24.979	1.64	0.062
0.00000007	0.016	0.533			1.64	0.068
0.00000005	0.019	0.367			1.67	0.062
0.00000006	0.038	0.490			1.68	0.068
0.00000005	0.016	0.509			1.63	0.059
0.00000005	0.017	0.499			1.62	0.073
0.00000005	0.016	0.302			1.64	0.07
0.00000006	0.020	0.504			1.61	0.074
0.00000005	0.016	0.489			1.72	0.071
0.00000006	0.016	0.506			1.66	0.076
0.00000006	0.034	0.273			1.69	0.066
0.00000004	0.035	0.494	-7.668	24.441	1.59	0.076
0.00000005	0.023	0.394	-6.656	23.124	1.67	0.078
0.00000005	0.033	0.424	-6.531	24.722	1.59	0.08
0.00000004	0.019	0.317	-7.291	23.139	1.66	0
0.00000005	0.025	0.368	-7.515	23.277	1.67	0.097
0.00000005	0.021	0.368	-7.56	23.48	1.66	0.092
0.00000004	0.026	0.394	-7.823	22.697	1.66	0.092
0.00000005	0.071	0.447	-7.524	23.701	1.69	0.087
0.00000004	0.112	0.694	-7.782	22.613	1.62	0.076
0.00000004	0.217	0.542	-7.435	21.576	1.64	0.078
0.00000004	0.371	0.563	-7.376	22.255	1.61	0.099
0.00000004	0.517	0.537	-7.194	23.119	1.57	0.063
0.00000003	0.533	0.558	-7.38	22.36	1.61	0.079
0.00000003	0.837	0.356	-7.106	22.984	1.56	0.079
0.00000004	0.839	0.292	-7.033	23.367	1.59	0.085
0.00000003	0.829	0.335	-6.799	23.579	1.52	0.086
0.00000003	0.720	0.432	-6.855	23.935	1.63	0.102
0.00000003	0.828	0.362	-7.015	24.063	1.61	0.116
0.00000004	0.733	0.296	-6.99	23.612	1.59	0.097
0.00000002	0.721	0.330	-6.786	22.988	1.61	0.109
0.00000002	0.696	0.309			1.62	0.098

0.00000002	0.639	0.308	-6.639	23.485	1.60	0.026
0.00000002	0.877	0.265			1.62	0.087
0.00000002	0.089	1.399	-6.978	21.957	1.56	0.087
0.00000002	1.127	0.230	-6.368	24.528	1.59	0.108
0.00000002	1.151	0.235	-5.606	24.99	1.54	0.078
0.00000003	1.256	0.156	-4.554	25.498	1.56	0.085
0.00000003	1.454	0.205	-4.839	25.863	1.57	0.124
0.00000003	1.403	0.072	-5.133	33.932	1.58	0.121
0.00000003	1.731	-0.040	-4.032	25.031	1.54	0.054
0.00000003	1.622	0.108	-3.783	26.078	1.54	0.133
0.00000003	1.767	0.256	-3.726	26.267	1.54	0.089
0.00000003	2.005	0.405	-4.186	25.83	1.53	0.1
0.00000002	1.938	0.356	-3.754	25.852	1.55	0.086
0.00000003	2.498	0.069	-3.614	26.557	1.54	0.051
0.00000003	1.817	0.423	-3.934	24.69	1.52	0.092
0.00000004	1.749	0.451	-4.388	25.24	1.57	0.102
0.00000004	1.947	0.321	-3.833	25.634	1.39	0.107
0.00000004	1.682	0.592	-3.89	24.897	1.38	0.08
0.00000004	1.718	0.389	-3.709	27.287	1.43	0.116
0.00000004	1.511	0.450	-4.722	25.268	1.34	0.111
0.00000005	1.495	0.418	-4.514	24.805	1.38	0.118
0.00000005	1.091	0.408	-4.582	24.454	1.38	0.123
0.00000005	0.447	0.341	-5.885	25.221	1.42	0.127
0.00000005	0.591	0.277	-6.301	25.193	1.36	0.126
0.00000005	0.431	0.268	-6.963	21.43	1.40	0.116
0.00000006	0.146	0.405	-5.944	28.269	1.40	0.118
0.00000005	0.140	0.212	-5.442	27.165	1.37	0.048
0.00000004	0.142	0.250	-5.382	27.587	1.40	0.107
0.00000007	0.144	0.259	-5.286	27.719	1.39	0.153
0.00000006	0.138	0.340	-5.129	26.687	1.38	0.099
0.00000004	0.136	0.173	-5.543	26.488	1.40	0.098
0.00000004	0.137	0.192	-5.538	26.848	1.37	0.112
0.00000006	0.194	0.137			1.25	0.143
0.00000006	0.196	0.297	-5.021	31.444	1.33	0.164
0.00000003	0.194	0.145	-4.978	26.235	1.34	0.084
0.00000003	0.197	0.163	-4.744	28.292	1.56	0.067
0.00000005	0.193	0.151	-5.59	29.833	1.45	0.079
0.00000003	0.193	0.273	-5.267	27.767	1.34	0.104
0.00000003	0.193	0.143	-5.937	29.133	1.52	0.1
0.00000002	0.194	0.171	-5.044	28.205	1.52	0.079
0.00000002	0.194	0.163	-4.448	26.61	1.49	0.067
0.00000002	0.194	0.406			1.48	0.071

0.00000003	0.192	0.402	-6.145	28.525	1.35	0.06
0.00000002	0.192	0.397	-8.798	35.113	1.39	0.115
0.00000004	0.216	0.400	-6.707	34.438	1.33	0.088
0.00000008	0.438	0.419	-6.702	28.912	1.16	0.11
0.00000005	0.395	0.415	-7.141	26.741	1.30	0.092
0.00000004	0.319	0.432	-7.176	28.701	1.34	0.076
0.00000004	0.281	0.400	-7.396	28.67	1.35	0.078
0.00000002	0.238	0.396	-7.369	33.403	1.43	0.087
0.00000001	0.207	0.384	-6.109	26.275	1.55	0.058
0.00000002	0.154	0.447	-6.437	29.651	1.52	0.033
0.00000002	0.190	0.412	-7.014	30.611	1.44	0.057
0.00000003	0.166	0.390	-6.896	34.436	1.45	0.07
0.00000013	0.143	0.400	-5.704	28.121	1.30	0.072
0.00000012	0.313	0.399	-6.344	28.803	1.20	0.103
0.00000012	0.151	0.409	-5.809	32.548	1.24	0.095
0.00000012	0.210	0.383	-6.931	24.249	1.25	0.108
0.00000013	0.186	0.432	-7.004	22.953	1.29	0.077
0.00000014	0.154	0.398	-6.359	23.307	1.40	0.032
0.00000014	0.214	0.343	-6.118	22.683	1.37	0.06
0.00000014	0.207	0.336	-6.036	23.25	1.45	0.03
0.00000014	0.240	0.242	-6.401	23.486	1.36	0.051
0.00000012	0.223	0.247	-6.072	23.803	1.23	0.048
0.00000014	0.222	0.252	-5.344	23.341	1.37	0.063
0.00000013	0.263	0.238	-5.848	24.363	1.28	0.098
0.00000012	0.223	0.279	-7.951	19.091	1.18	0.105
0.00000013	0.215	0.275	-5.454	24.011	1.33	0.059
0.00000014	0.191	0.268	-6.605	23.771	1.45	0.042
0.00000015	0.195	0.234	-6.785	22.774	1.47	0.04
0.00000015	0.193	0.188	-6.686	23.048	1.46	0.038
0.00000015	0.188	0.191			1.47	0.034
0.00000015	0.188	0.185	-6.024	25.305	1.51	0.025
0.00000015	0.189	0.230	-6.563	23.408	1.49	0.024
0.00000014	0.188	0.230			1.44	0.022
0.00000015	0.188	0.250			1.47	0.025
0.00000015	0.190	0.246	-6.444	21.176	1.48	0.025
0.00000014	0.167	0.227	-6.675	23.382	1.44	0.026
0.00000015	0.169	0.290	-6.41	26.974	1.49	0.024
0.00000014	0.186	0.265	-5.998	23.94	1.45	0.028
0.00000014	0.190	0.243	-5.769	23.265	1.42	0.028
0.00000014	0.173	0.258	-6.585	19.384	1.43	0.027
0.00000014	0.186	0.261	-6.056	23.88	1.42	0.03
0.00000014	0.205	0.262	-5.734	24.403	1.42	0.031

0.00000014	0.192	0.268	-5.966	24.158	1.35	0.041
0.00000013	0.169	0.362	-6.661	24.428	1.30	0.039
0.00000012	0.184	0.279	-5.425	27.367	1.18	0.02
0.00000009	0.445	0.221	-6.25	24.855	0.93	0.229
0.00000010	0.294	0.265	-6.612	24.855	1.02	0.186
0.00000011	0.230	0.345	-5.707	23.907	1.07	0.258
0.00000012	0.235	0.312	-5.995	23.027	1.22	0.14
0.00000014	0.221	0.303	-6.155	22.752	1.38	0.065

VITA

Morgan Ostroski

Candidate for the Degree of Geology

Master of Science

Thesis: INVESTIGATING THE FORMATION AND EVOLUTION OF MEGA-PALEOLAKES IN THE MIDDLE KALAHARI OF SEMI-ARID BOTSWANA FROM SEDIMENTARY AND GEOCHEMICAL PROXIES

Major Field: Geology

Biographical:

Education:

Completed the requirements for the Master of Science in Geology at Oklahoma State University, Stillwater, Oklahoma in May, 2013.

Completed the requirements for the Bachelor of Science in Geology at Mercyhurst College, Erie, PA in 2011.

Experience:

Boone Pickens School of Geology Teaching Assistantship (2011-2013)
Geology Intern – EOG Resources (May-Aug. 2012)

Professional Memberships:

American Association of Petroleum Geologists
Geological Society of America